Particulate matter stoichiometry driven by microplankton community structure in summer in the Indian sector of the Southern Ocean

M. Rembauville, S. Blain, J. Caparros, I. Salter

Particulate matter stoichiometry driven by microplankton community structure in summer in the Indian sector of the Southern Ocean

M. Rembauville[1], S. Blain[1], J. Caparros[1], I. Salter[1,2].

[1]Sorbonne Universités, UPMC Univ Paris 06, CNRS, Laboratoire d'Océanographie Microbienne (LOMIC), Observatoire Océanologique, F-66650, Banyuls/mer, France

[2]AlfredWegener Institute, Helmholtz Centre for Polar and Marine Research, Am Handelshafen 12, 27570 Bremerhaven, Germany

Corresponding author: M. Rembauville (rembauville@obs-banyuls.fr)

Southern Ocean – Microplankton – Particulate stoichiometry – Subsurface chlorophyll maxiumum – Nutrient diffusion

Abstract

Microplankton community structure and particulate matter stoichiometry were investigated in a late summer survey across the Subantarctic and Polar Front in the Indian sector of the Southern Ocean. Microplankton community structure exerted a first order control on PON:POP stoichiometry with diatom-dominated samples exhibiting much lower ratios (4 – 6) than dinoflagellate and ciliate-dominated samples (10 – 21). A significant fraction of the total chlorophyll *a* (30 - 70%) was located beneath the euphotic zone and mixed layer and sub-surface chlorophyll features were associated to transition layers. Although microplankton community structure and biomass was similar between mixed and transition layers, the latter was characterized by elevated Chl:POC ratios indicating photoacclimation of mixed layer communities. Empty diatom frustules, in particular of *Fragilariopsis kerguelensis* and *Pseudo-nitzschia*, were found to accumulate in the Antarctic Zone transition layer and were associated to elevated BSi:POC ratios. Furthermore, high $Si(OH)_4$ diffusive fluxes (>1 mmol m^2 d^{-1}) into the transition layer appeared likely to sustain silicification. We suggest transition layers as key areas of C and Si decoupling through (i) physiological constraints on carbon and

29 silicon fixation (ii) as active foraging sites for grazers that preferentially remineralize carbon.
30 On the Kerguelen Plateau, the dominant contribution of *Chaetoceros Hyalochaete* resting
31 spores to microplankton biomass resulted in a three-fold enhancement of POC concentration
32 at 250 m, compared to other stations. These findings further highlight the importance of
33 diatom resting spores as a significant vector of carbon export through the intense
34 remineralization horizons characteristing Southern Ocean ecosystems.

Introduction

The Southern Ocean connects the three major Ocean basins and is important for heat and carbon exchange with the atmosphere, representing a critical conduit by which anthropogenic CO_2 enters the ocean (Sabine et al. 2004; Khatiwala et al. 2009). Modeling studies have suggested that nutrients exiting the Southern Ocean, through the formation of mode water, may constrain primary production in vast areas of the global Ocean (Sarmiento et al. 2004; Dutkiewicz et al. 2005). The efficiency and stoichiometry of surface nutrient depletion by the biological pump in the Southern Ocean can thus have major implications for global Ocean productivity (Primeau et al. 2013). A large fraction of present-day Southern Ocean surface waters are referred to as "High-Nutrient, Low-Chlorophyll" areas (HNLC, Minas et al. 1986) where low trace-metal concentrations, in particular iron, can limit primary production (Martin 1990; de Baar 1990) and result in a weaker biological pump (e.g. Salter et al. 2012). Regional trace metal inputs from shelf sediments and glacial melt-water can sustain large scale (100 km) and long lasting (several months) phytoplankton blooms in proximity to island systems such as South Georgia, Crozet and Kerguelen plateaus (Whitehouse et al. 2000; Blain et al. 2001; Pollard et al. 2007).

Many studies of phytoplankton blooms in the Southern Ocean usually focus on the euphotic zone and studies using satellite data (e. g. Park et al. 2010; Borrione and Schlitzer 2013) are restricted to the surface. However, subsurface chlorophyll maxima (SCM) deeper than the euphotic zone at the base of the mixed layer are recurrent in late summer in the HNLC waters of the Southern Ocean (Parslow et al. 2001, Holm-Hansen and Hewes 2004; Holm-Hansen et al. 2005). Sub-surface chlorophyll features were also observed over the productive central Kerguelen Plateau in late summer (February) with chlorophyll *a* concentrations >2.5 µg L^{-1} (Uitz et al. 2009), suggesting that SCM are not strictly restricted to the HNLC waters. These sub-surface biomass features are observed around 100 m and thus

escape satellite detection depth (~20 m in productive areas; Gordon and McCluney 1975). This region of the water column, also called the "transition layer", is defined as the interface between the stratified ocean interior and the highly turbulent surface mixed layer (Johnston and Rudnick 2009).

Diatoms typically dominate spring/summer phytoplankton blooms in the Southern Ocean (Korb and Whitehouse 2004; Armand et al. 2008; Quéguiner 2013), and the subsurface chlorophyll maximum is also characterized by a dominance of diatom biomass (Kopczynska et al. 2001; Armand et al. 2008; Gomi et al. 2010). Both studies from Armand et al. (2008) and Gomi et al. (2010) described a similarity between the mixed layer and deep diatom communities. However, Kopczynska et al. (2001) reported a difference between the mixed layer and the subsurface phytoplankton diatom assemblage with a dominance of larger species in the deeper samples. Additionally, high regional and inter-annual variability of diatom assemblages in the SCM is reported from two consecutive summer surveys in the Polar Frontal Zone and the Seasonal Ice Zone in the Indian Sector of the Southern Ocean (Gomi et al. 2010).

It has been proposed that the development of sub-surface biomass features in the Southern Ocean is linked to iron depletion in the mixed layer (Parslow et al. 2001). Under these conditions, phytoplankton accumulates in temperature minimum layers that are frequently associated to the pycnocline and/or nutricline (Holm-Hansen and Hewes 2004). The similarity that is frequently observed between mixed layer and the SCM diatom communities supports this hypothesis (Armand et al. 2008; Gomi et al. 2010). It is presently unclear, however, if the SCM phytoplankton communities are predominantly senescent and/or poorly active (Parslow et al. 2001; Armand et al. 2008) or productive communities with low growth rates sustained by nutrient diffusion through the pycnocline (Holm-Hansen and Hewes 2004; Quéguiner 2013). Irrespective of photosynthetic production levels, it has been

suggested previously that the transition layer could be an important foraging site for various micro- and mesozooplanktonic grazers (Kopczynska et al. 2001; Gomi et al. 2010). A coupled study of microplankton assemblages and particulate matter stoichiometry is therefore of particular importance to gain a better understanding of SCM formation and their impact on carbon and biomineral cycling through transition layers in the Southern Ocean.

Redfield (1958) first described the homogeneity of deep water N and P stoichiometry and its coherence with plankton stoichiometry and the resulting "Redfield-ratio" has been a central tenet in modern oceanography. The quantity of particulate matter data has increased substantially in recent years and stoichiometric nutrient ratios are commonly observed to derivate from Redfield values. A recent large scale data synthesis demonstrated that PON:POP ratios are not homogeneous at a global scale and may reflect latitudinal patterns related to plankton community composition (Martiny et al. 2013). Diatoms, for example, are known to have a lower N:P ratio than dinoflagellates or chlorophyceae (Quigg et al. 2003; Ho et al. 2003; Sarthou et al. 2005).

There are alternative explanations for latitudinal trends in particulate matter stoichiometry. The growth rate hypothesis (Elser et al. 1996) suggests that among one phytoplankton taxa, changes in physiological status affects the allocation of nutrients to various macromolecular pools with different N:P stoichiometry. For example, competitive equilibrium in nutrient limiting conditions will lead to the synthesis of N-rich proteins required for nutrient acquisition. During exponential growth, there is an increased demand for the synthesis of P-rich ribosomes which are required for cell component synthesis. (Elser et al. 1996; Sterner and Elser 2002; Klausmeier et al. 2004). This general scheme might be modulated by local availability of nutrients, and phytoplankton for example have been reported to synthesize non-phosphorous lipids in oligotrophic, low P environments (Van Mooy et al. 2009). Temperature has also been identified as a factor strongly influencing the

110 N:P ratios and Southern Ocean diatoms contain more P-rich rRNA at low temperatures
111 (Toseland et al. 2013). These observations reinforce the need of a joint description of
112 plankton community structure and stoichiometry to document how plankton biogeography
113 might impact Southern Ocean nutrient stoichiometry at local scale (Weber and Deutsch 2010).

114 In the present study, we report data acquired late summer in the Subantarctic Zone, the
115 Polar Frontal Zone, and the Antarctic Zone in the Indian Sector of the Southern Ocean. Our
116 objectives are (1) to assess whether patterns in sub-surface chlorophyll features are linked to
117 biomass accumulation at physical interfaces, (2) to compare microplankton assemblages
118 between the mixed layer and transition layer and identify physiological changes and potential
119 ecological processes occurring within the transition layer, (3) investigate the statistical
120 relationship between microplankton community structure and particulate matter stoichiometry
121 in contrasting hydrological environments, and (4) to assess how biogeochemical processes
122 within the transition layer modulate the intensity and stoichiometry of the particulate matter
123 transfer from the mixed layer to the mesopelagic ocean.

124 **Material and Methods**

125 **OISO23 cruise and sampling strategy**

126 The OISO23 cruise took place onboard the R/V *Marion Dufresne* in the Indian sector of the
127 Southern Ocean from the 6 January to the 23 February 2014. The biogeochemical study
128 presented here is focused on 11 stations located on a latitudinal transect in the Subantarctic
129 Zone (SAZ), Polar Frontal Zone (PFZ) and Antarctic Zone (AAZ), linking the two island
130 systems of Crozet and Kerguelen (Fig. 1, Table 1). Conductivity-Temperature-Depth (CTD,
131 Seabird SBE 911 plus) casts were performed at each station. Samples for nutrients and
132 chlorophyll *a* analyses were taken at 20 fixed depths. Precise sampling depths for particulate
133 matter and microplankton abundance were chosen at each station following a preliminary
134 analysis of the down-cast temperature, salinity and fluorescence profiles. Samples were taken

in the mixed layer, in the strong density gradient beneath the mixed layer (transition layer) and at a constant depth of 250 m. The last depth was chosen as a reference depth located under the annual upper mixed layer for this sector of the Southern Ocean (Park et al. 1998; de Boyer Montégut et al. 2004).

Derived hydrological parameters

The turbulent diffusivity coefficient was computed with the Thorpe scale method using the Shih et al. (2005) parameterization as previously described in Park et al. (2014). The robustness of the Thorpe scale calculation using this indirect method depends on the level of CTD processing prior to the computation (Park et al. 2014). The diffusivity coefficient (Kz in $m^2\ s^{-1}$) was calculated as follows:

$$Kz = 1.6\ \nu^{1/2}\ L_t\ N^{1/2} \qquad (1)$$

where ν is the cinematic viscosity of seawater ($1.5 – 1.8\ 10^{-6}\ m^2\ s^{-1}$ for T = 0 to 5 °C), L_t is the Thorpe scale (vertical density overturning scale, in m) and N is the Brunt-Väisalä buoyancy frequency (s^{-1}) defined as :

$$N = \left(-\frac{g}{\rho_e} \times \frac{d\rho}{dz}\right)^{1/2} \qquad (2)$$

where g is the gravitational acceleration ($9.81\ m\ s^{-1}$), ρ_e is a constant reference density for seawater, ρ is the seawater density and z is the depth (m). Brunt-Väisälä buoyancy frequency was used to quantify the water column stability and the strength of the physical interface associated with the transition layer. Each *Kz* profile was averaged in 10 m bins. The Thorpe scale method cannot resolve overturns smaller than 20 cm, consequently Kz values $<10^{-5}\ m^2\ s^{-1}$ were set to this minimal value based on in situ measurements around the Kerguelen plateau with a Turbo MAP profiler (Park et al. 2014).

157 The mixed layer depth (MLD) was calculated using a 0.02 kg m^{-3} density-difference
158 criterion relative to the density at 20 m (Park et al. 1998). The depth of the euphotic layer (Ze,
159 1% of the surface irradiance, in m) was calculated from the vertical profile of fluorescence-
160 derived chlorophyll *a* using Morel and Berthon (1989) formulation:

161 $$Ze = 568.2\ (\int_0^z chla\ dz)^{-0.746} \qquad (3)$$

162 where *chla* is the chlorophyll *a* concentration (mg m^{-3}) derived from the calibrated CTD
163 fluorometer (WET Labs ECO FL, see below for calibration method). The calculation was
164 performed iteratively downward from the surface until *z* = *Ze*.

165 **Biogeochemical analyses**

166 **Particulate matter: particulate organic carbon (POC), nitrogen (PON),**
167 **phosphorous (POP), biogenic silica (BSi) and chlorophyll *a* analysis**

168 For POC and PON, 2 L of seawater were filtered on precalcinated (450°C, 24 h) 25 mm
169 Whatman GF/F filters stored in precalcinated glass vials and dried overnight at 60 °C. Filters
170 were decarbonated by fumigating pure HCl (Merck) during 10 h. POC and PON were
171 measured on a Perkin Elmer C,H,N 2400 autoanalyser calibrated with acetanelyde. Detection
172 limits were defined as the mean blank plus three times the standard deviation of the blanks
173 and were 0.17 and 0.04 µmol L^{-1} for POC and PON, respectively. For POP, 500 mL of
174 seawater was filtered on precalcinated GF/F filters. POP was analyzed following a wet
175 oxidation procedure (Pujo-Pay and Raimbault 1994). Extracts were filtered through two
176 precalcinated GF/F filters prior to spectrophotometric analysis of PO_4^{3-} on a Skalar
177 autoanalyser following the method of Aminot and Kerouel (2007). The detection limit for
178 POP was 0.01 µmol L^{-1}.

179 For BSi, 1 L of seawater was filtered on 25 mm nuclepore filter of 0.2 µm porosity.
180 Filters were placed in cryotubes and dried at 60 °C overnight. BSi was estimated by the triple

NaOH/HF extraction procedure allowing correction of lithogenic silica (LSi, Ragueneau et al. 2005). Filters were digested two times with 0.2 N NaOH at 95 °C during 45 min. At the end of both extractions, aliquots were taken for silicic acid ($Si(OH)_4$) and aluminum (Al) concentration measurements. A third extraction was performed with 2.9 N HF over 48 h at ambient temperature (~20 °C). $Si(OH)_4$ was determined colorimetrically on a Skalar autoanalyser following Aminot and Kerouel (2007) and Al was determined fluorimetrically using the Lumogallion complex (Howard et al. 1986). The detection limit for BSi was 0.02 µmol L^{-1}. The LSi correction was most important in the vicinity of the plateaus (e.g. at A3, 250 m the LSi represented 17% of the total particulate Si).

For chlorophyll *a* analysis, 2L of seawater were collected in opaque bottles, filtered onto GF/F filters and immediately placed in cryotubes at -80 °C. Pigments were extracted in 90% acetone solution and analyzed using 24 fluorescence excitation and emission wavelengths with a Hitachi F-4500 fluorescence spectrophotometer according to Neveux and Lantoine (1993). These chlorophyll *a* concentrations measured from niskin bottles were used to calibrate the CTD fluorescence profiles by linear regression ($R^2 = 0.8$).

Dissolved nutrients analysis and calculation of diffusive fluxes

For the analysis of major nutrients (NO_3^-, NO_2^-, $Si(OH)_4$, PO_4^{3-}), 20 mL of filtered (0.2 µm cellulose acetate filters) seawater was sampled into scintillation vials and poisoned with 100 µL of 100 mg L^{-1} $HgCl_2$. Nutrient concentrations were determined colorimetrically on a Skalar autoanalyzer following Aminot and Kerouel (2007). Nutrient gradients were calculated at each sampling depth for particulate matter and microplankton based on the three nutrient concentrations (*C*) windowing this depth. Nutrient diffusive fluxes (N_{diff} in µmol m^{-2} s^{-1}) in the transition layer were calculated as follow:

$$N_{\text{diff}} = Kz\frac{dC}{dz} \qquad (4)$$

Kz profiles are highly variable over short time scales (days to hour), whereas nutrient gradients result from nutrient consumption occurring at longer timescales (weeks to month). To minimize the bias caused by short term Kz variability, nutrient diffusive fluxes were calculated using the average Kz profile from the study region (supplementary Figure 1). A characteristic value of 4.5×10^{-5} m^2 s^{-1} in the transition layer was derived from the mean Kz profile.

Microplankton abundance, identification and biomass calculation

Seawater samples for microplankton identification and enumeration were collected in 125 mL amber glass bottles and immediately fixed with acid Lugol solution (1% final concentration). Samples were maintained in the dark at ambient temperature until counting (performed within three months after the sampling). Microplankton cells were enumerated from either a 50 mL (mixed layer and transition layer) or 100 mL (250 m) subsample after settling for 24 hours (dark) in an Utermöhl counting chamber. Taxonomic identification was performed under an inverted microscope (Olympus IX71) with phase contrast at 200x and 400x magnification. One half of the counting chamber (mixed layer and transition layer) or the entire surface (250 m samples) was used to enumerate the microplankton. The total number of cells counted was >200 except in sample 13 at 250 m. Ciliates and tintinnids were enumerated but not classified into taxa. Dinoflagellates were identified to the genus level, and diatoms were identified to species level when possible, following the recommendations of Hasle and Syvertsen (1997). Full and empty diatoms frustules were enumerated separately. Half or broken frustules were not considered. Due to the preserved cell contents sometimes obscuring taxonomic features on the valve face, taxonomic identification of diatoms to the species level was occasionally difficult and necessitated the categorizing of diatom species to genus or taxa as previously described in Rembauville et al. (2015a).

The composition of living diatom biomass was estimated from the abundance of full cells using a species-specific carbon content for diatoms in the Indian sector of the Southern Ocean (Cornet-Barthaux et al. 2007). For species absent from this reference, >20 individuals were measured from microscopic images using the imageJ software. Cell volume for the appropriate shape was calculated following Hillebrand et al. (1999) and carbon content was calculated using a diatom-specific carbon:volume relationship (Menden-Deuer and Lessard 2000). The same procedure was used for dinoflagellates and ciliates. For *Chaetoceros Hyalochaete* resting spores (CRS), the carbon content for spores over the Kerguelen plateau calculated in Rembauville et al. (2015a) was used. A complete list of microplankton categories and their respective carbon content is provided in Supplementary Table 1.

Statistical analyses

To compare microplankton community structure between samples, Bray-Curtis distance was calculated based on raw microplankton abundances. Samples were clustered using the unweighted pair group method with arithmetic mean (UPGMA). To link microplankton community structure with biogeochemical factors (particulate matter stoichiometry and nutrient diffusive fluxes), a canonical correspondence analysis (CCA) was performed (Legendre and Legendre 1998). Prior to the CCA, microplankton abundances were sorted into groups to facilitate the ecological interpretation of the analysis. For example, a distinction is often made between small and large diatoms that are thought to occupy different niches of nutrient and light availability, and have different sensitivity to grazing in the Southern Ocean (Smetacek et al. 2004; Quéguiner 2013). “Large diatoms (>100 µm)” comprised the following genera: *Corethron, Dactyliosolen, Membraneis, Pleurosigma, Proboscia, Rhizosolenia* and *Thalassiothrix*. “Small diatoms (<100 µm)” referred to the other diatom genera. Armored dinoflagellates (*Prorocentrum, Ceratium, Brachidinium, Dinophysis, Oxytoxum, Podolampas*

and *Protoperidinium)* were differentiated from naked dinoflagellates (*Gymnodinium* and *Gyrodinium*).

Results

Hydrological characteristics and nutrients diffusive flux

During the study (11 January to 8 February), the north Crozet bloom had terminated and partly advected by mesoscale features of the SAF associated with strong geostrophic velocities (Fig. 1). Surface waters of the PFZ displayed very low chlorophyll *a* concentration (<0.3 µg L^{-1}) and the bloom of the central Kerguelen plateau was also declining (~0.8 µg L^{-1}). East of Kerguelen Island, on the northern flank of the PF, a chlorophyll *a* plume originating from coastal waters was advected eastward as the PF merged with the SAF. A potential temperature-salinity diagram (Fig. 2) was used to classify the different stations into discrete hydrological zones, summarized in Table 1. The Subantarctic Zone (SAZ) displayed the highest surface temperatures (>10°C, stations 5, 13 and 14). The Polar Frontal Zone (PFZ) exhibited a clear decrease in surface salinity (<34, stations 6, 7, 8 and 12) and the Antarctic Zone (AAZ) was characterized by the presence of a temperature minimum layer (~1.8 °C; stations 9, 10, 11 and A3). The Si* (= $Si(OH)_4 – NO_3^-$) in intermediate and winter waters was homogeneous (~0 µmol L^{-1}) at all stations. Therefore, the Si* signature of surface waters was used as a tracer for $Si(OH)_4$ uptake relative to nitrate in the productive layer, rather than differences in preformed nutrients. In the SAZ, Si* was similar in surface water and intermediate waters (0 µmol L-1) whereas in the PFZ and the AAZ, Si* in surface waters was strongly negative (<-20 µmol L-1).

At all stations, 30-70% of the vertically integrated chlorophyll *a* occurred deeper than the MLD (Table 2). However, only stations 6, 9, 12, 13 and 14 exhibited a maximum chlorophyll *a* concentration deeper than the MLD. Brunt-Väisälä frequencies (*N*) were highest in the transition layer and ranged from 4.5-8.2 cycles h^{-1}, with high values associated with

frontal (e.g. station 13 close to SAF) or bathymetric (station 6 near the Crozet plateau) structures. At stations located close to the Kerguelen plateau (9, 10 and A3), Ze was shallower than the MLD. Station 9 displayed a characteristic subsurface chlorophyll maximum where chlorophyll *a* shows a steep increase under the MLD (70 m) and a gradual decrease in the pycnocline down to 150 m (Fig. 3). Kz values peak at 9.5×10^{-5} m^2 s^{-1} in the mixed layer but display a second maximum associated with the pycnocline, nutriclines, and elevated chlorophyll *a* values of 1.1 µg L^{-1}. The gradient between 150 m and the mixed layer was much higher for $Si(OH)_4$ (20 µmol L^{-1} to <2 µmol L^{-1}) than for NO_3^- (27 µmol L^{-1} to 23 µmol L^{-1}) and PO_4^{3-} (2.2 µmol L^{-1} to 1.5 µmol L^{-1}).

Nutrient gradients estimated for the three different layers covered two order of magnitude and were generally larger for $Si(OH)_4$ (Table 2). Highest $Si(OH)_4$ gradients (>200 µmol m^{-4}) were observed in the transition layer in stations of the AAZ close to the Kerguelen plateau (stations 9, 10, A3), leading to large $Si(OH)_4$ diffusive fluxes (≥1 mmol m^{-2} d^{-1}). Highest NO_3^- gradients (~100 µmol m^{-4}) were found in the transition layer of stations 5 and 6 close to the Crozet Island, associated with the highest NO_3^- diffusive fluxes (>300 µmol m^{-2} d^{-1}). PO_4^{3-} gradients were at least one order of magnitude lower (<10 µmol m^{-4}) than nitrate gradient, resulting in negligible diffusive fluxes.

Particulate matter stocks and stoichiometry

POC concentrations generally decreased with depth with highest values found in the mixed layer of the SAZ (> 10 µmol L^{-1}), followed by the AAZ (4.4-9.1 µmol L^{-1}) and PFZ (4.5-6.0 µmol L^{-1}, Table 2). The largest value of 18.6 µmol L^{-1} at station 5 corresponded to a biomass patch in a meander of the SAF (Fig. 1). POC concentrations in the transition layer ranged from 2.7 to 8.2 µmol L^{-1} with the highest value observed over the Kerguelen plateau (Station A3). At the reference depth of 250 m POC concentrations were relatively uniform (1.4 ± 0.3

302 µmol L^{-1}), although on the Kerguelen plateau (Station A3) they were notably higher (3.4
303 µmol L^{-1}).

304 The highest chlorophyll *a* concentration was observed in the warm mixed layer of
305 station 5 (1.26 µg L^{-1}). Stations in the PFZ exhibited the lowest mixed layer chlorophyll *a*
306 concentrations (0.40 - 0.50 µg L^{-1}), intermediate values were found in the SAZ (0.60 – 0.90
307 µg L^{-1}) and highest values in the AAZ (~ 1 µg L^{-1}). Unlike POC, chlorophyll *a* values in the
308 transition layer frequently exceeded those in the mixed layer, with the largest value of 1.20 µg
309 L^{-1} observed at the Kerguelen plateau station A3. Similarly the largest 250 m POC
310 concentration of 0.21 µg L^{-1} was observed at station A3, compared to negligible values of <
311 0.05 µg L^{-1} at all other stations.

312 All the samples from the SAZ and PFZ displayed BSi:POC ratios <0.2 (Fig. 4).
313 Conversely, in the AAZ, BSi:POC values were between 0.4 and 0.9 with highest values found
314 in the transition layers. POC:PON ratios generally displayed a typical increase with depth
315 with a notable exception at station A3 (Kerguelen plateau) where the POC:PON ratio was
316 vertically homogeneous (6.3). PON:POP ratios demonstrated more variability than
317 POC:PON. In the AAZ, PON:POP mixed layer ratios were between 4-8, increasing with
318 depth. Mixed layer values in the PFZ (stations 6-10) were slightly higher than the AAZ (6-9),
319 and SAZ samples were notably larger with values >10. The highest values of 16-21 were
320 found in transition layer PFZ samples located between the Crozet and Kerguelen Islands
321 (stations 6, 7, and 8). Chl:POC ratio (g g^{-1}) were generally highest in the transition layer and
322 lowest in 250 m samples. The largest Chl:POC ratios of 0.016-0.018 were observed in the
323 transition layer of the AAZ.

324 **Microplankton abundance and distribution**

325 The largest microplankton cell abundance (527 × 10^3 cell L^{-1}) was observed in the mixed
326 layer of station 5 and corresponded to a community dominated (>90%) by *Bacteriastrum* spp.

(Table 3), constituting the external branch of the dendrogram based on Bray-Curtis distance (Fig. 5). The low biomass group A (<50 $\times 10^3$ cell L^{-1}) contained the subgroup C which represented mixed layer and transition layer of PFZ stations 6 and 12 characterized by an equal proportion of full diatoms (>100 µm), *Prorocentrum* and naked ciliates. Subgroup D contained all of the 250 m samples (except A3) and transition layer samples from the PFZ stations 7 and 8, the latter characterized in decreasing order by empty diatoms (<100 µm), *Prorocentrum* and naked ciliates. Group B (high abundance) contained three subgroups, E, F and G. Subgroup E represented the majority of surface and transition layer samples from the AAZ and was characterized by a strict dominance of full diatoms (<100 µm). Subgroup F constituted samples from the mixed and transition layer of SAZ stations 13 and 14 with an assemblage of *Prorocentrum* and full diatoms (<100 µm). Finally, subgroup G contained samples from the transition layer and deep layer at A3 dominated by *Chaetoceros Hyalochaete* resting spores and full diatoms (<100 µm). It is generally stated that bottle sampling might under-sample large and rare diatoms (Armand et al. 2008). Therefore our data might underestimate the contribution of large diatoms to the total microplankton assemblage.

The fraction of empty diatoms generally increased with depth (up to 90 % at 250 m in the PFZ), with the notable exception of station A3 where it remained ~20%. *Fragilariopsis kerguelensis* dominated (>60 %) the empty diatoms in all the samples of the AAZ and PFZ at any depth, with the exception of station A3 (Fig. 6). Station 5 was mostly characterized by empty *Bacteriastrum* spp. cells. In stations 13 and 14 (SAZ) the mixed layer empty diatom community was dominated by *Pseudo-nitzschia* spp., *Thalassiothrix antarctica* and *Chaetoceros Hyalochaete* (vegetative). Mixed layer sample at A3 contained in decreasing abundance empty cells of *F. kerguelensis*, *Pseudo-nitzschia* spp., *Eucampia antarctica* var. *antarctica* and *Corethron* spp. In the transition layer of stations 13 and 14 (SAZ), empty diatoms were dominated by *C. Hyalochaete* (vegetative) and *Pseudo-nitzschia* spp. At A3,

empty diatoms in the transition layer were dominated by *Pseudo-nitzschia* spp. (50 %), followed by *C. Hyalochaete* (vegetative) and *E. antarctica* var. *antarctica*. Finally, empty *Pseudo-nitzschia* (45 %), *C. Hyalochaete* (vegetative, 18 %) and *F. kerguelensis* (12 %) were observed at 250 m at A3.

Microplankton POC partitioning

A highly significant linear correlation (Spearman, n = 33, ρ = 0.88, p <0.01) was found between the measured POC (Table 2) and the calculated total microplankton POC (POC_{micro}, Table 3). The regression slope (0.7), and significant intercept (~1 µmol L^{-1}), suggested that the microplankton biomass calculation underestimated the total POC. At station 5, the mixed layer sample was dominated by *Bacteriastrum* spp. (>60 %, Fig. 7). At stations 6 to 8 (PFZ between Crozet and Kerguelen), naked ciliates (>40 %) and dinoflagellates were the main contributors to POC_{micro} at any depth. In the mixed layer samples of stations 13 and 14 (SAZ) dinoflagellates dominated (>50 %) the POC_{micro}. In the AAZ, diatoms dominated POC_{micro} at all stations, with a major contribution of the assemblage of large diatoms (>100 µm): *Rhizosolenia* spp., *Corethron* spp., *T. antarctica, Membraneis* and *F. kerguelensis* (<100 µm). The same pattern of dominant taxa was also observed in the transition layer of the AAZ. At stations 12, 13 and 14 (north of Kerguelen), dinoflagellates followed by *Membraneis* and *Pseudo-nitzschia* spp were the main contributors to POC_{micro}. In the deep samples, POC_{micro} was dominated by the contribution of dinoflagellates (mainly *Prorocentrum*) and ciliate biomass with a noticeable exception at station A3 with the presence of *C. Hyalochaete* resting spores (>60 % POC_{micro}).

Particulate matter signature and microplankton assemblages

The first two axes of the CCA accounted for ~88 % of the variability within the dataset (Fig. 8). Axis 1 opposed AAZ and SAZ stations characterized by a dominance of diatoms and high BSi:POC stoichiometry to the PFZ stations dominated by dinoflagellates and ciliates and a

high PON:POP ratio. Axis 2 globally opposed surface samples with marked NO_3^- and PO_4^{3-} gradients associated with full diatoms (<100 µm) to the 250 m samples with a high POC:PON ratio associated with empty diatoms (<100 µm). Full diatoms (>100 µm) were projected close to the Chl:POC ratio and the AAZ transition layer samples. Finally, empty diatoms (>100 µm) were projected close to the $Si(OH)_4$ gradient, the BSi:POC ratio and the transition layer samples and deep samples of the AAZ.

Discussion

Microplankton community and physiology in the transition layer

During our study (January-February), the period of maximum productivity had already occurred (supplementary animation). The North Crozet bloom ended and was partly advected eastward in the Subantarctic Front (SAF), and the central Kerguelen plateau bloom was also in decline. Large and negative Si* values in the PFZ and AAZ (Fig. 2) suggested intense $Si(OH)_4$ utilization compared to nitrate utilization associated to bloom features. This can result from a dominance of diatoms in phytoplankton populations together with an increase in Si:N uptake ratio in response to iron limitation (Hutchins and Bruland 1998; Takeda 1998; Moore et al. 2007). Low concentrations of $Si(OH)_4$ (1.8 µmol L^{-1}; Mosseri et al. 2008) and dissolved iron (~0.1 nmol L^{-1}; Blain et al. 2008) over the central Kerguelen plateau in summer suggest that both elements may limit diatom growth in summer mixed layers.

The subsurface chlorophyll maximum is a recurrent feature in the oligotrophic ocean (Venrick et al. 1973; Letelier et al. 2004; Mignot et al. 2014), the North Sea (Weston et al. 2005), and the Arctic (Martin et al. 2010). The SCM can be associated with a phytoplankton biomass maximum (Martin et al. 2010), or the two structures can be uncoupled, suggesting that the vertical distribution of chlorophyll is strongly determined by photoaccliamtation (Fennel and Boss 2003). In the Southern Ocean, it has been proposed that the development of sub-surface biomass features is linked to such nutrient depletion, in particular iron in the

mixed layer (Parslow et al. 2001). Under these conditions, phytoplankton accumulates in temperature minimum layers that are frequently associated to the pycnocline and/or nutricline (Holm-Hansen and Hewes 2004). In the present study a large fraction of integrated chlorophyll *a* was observed below the mixed layer and the euphotic layer in the SAZ, PFZ and AAZ in the vicinity of the Crozet and Kerguelen plateaus. The transition layer constitutes a physical interface of increased water column stability, as diagnosed by maximum Brunt-Väisälä frequencies (Table 2). However, although POC and POC_{micro} concentrations were higher in the transition layer relative to the deep-reference samples, they were notably lower than those of the mixed layer (Table 2, 3), not indicative of biomass accumulation on this physical interface. Furthermore, examples of significant sub-surface biomass accumulation in the Southern Ocean have been associated to divergent diatom communities with an accumulation of larger diatoms at depth (Kopczynska et al. 2001). In our regional survey, mixed layer and transition layer diatom communities were similar, consistent with more localised studies (Armand et al. 2008; Gomi et al. 2010). The data presented above suggests that subsurface chlorophyll features are not necessarily associated with biomass accumulation in the Southern ocean and this is consistent across a broad spatial scale.

In the PFZ and AAZ, the highest Chl:POC ratios were observed in the transition layer and we suggest this is linked to photoacclimation. It is known that Chl:POC ratios of phytoplankton can cover more than one order of magnitude (0.003 – 0.055 g g^{-1}; Cloern et al. 1995) and due to photoacclimation vary fourfold among single diatom species (Anning et al. 2000). The CCA results highlight the association of high Chl:POC ratios with full and large (>100 µm) diatom cells in the transition layer of the AAZ. Southern Ocean diatoms have developed an acclimation strategy to low light and iron levels by increasing the amount of light-harvesting pigments on photosynthetic units, rather than multiplying the number of photosynthetic units (Strzepek et al. 2012).

427 It has been suggested previously that nutrient diffusion through the pycnocline could
428 sustain phytoplankton production in a transition layer when mixed layer nutrient
429 concentrations reach limiting levels (Holm-Hansen and Hewes 2004; Johnston and Rudnick
430 2009; Quéguiner 2013). There was no evidence of oxygen accumulation in the transition layer
431 (data not shown) suggesting minimal photosynthetic production, although diffusion and
432 heterotrophic respiration may have dampened an already low signal. Unfortunately no carbon
433 fixation data is available to validate the hypothesis of negligible photosynthetic rates below
434 the euphotic layer. However, production in the transition layer would also require iron
435 diffusion but ferriclines can be significantly deeper than mixed layers and transition layers.
436 On the Kerguelen plateau, although the transition layer occurs at 110 m, the ferricline is
437 located at 175 m in summer (Blain et al. 2008). This is a pattern generally applicable to the
438 Southern Ocean as a whole, where summer ferricline horizons appear to be systematically
439 deeper than mixed layer depths (Tagliabue et al. 2014) and thus significant carbon fixation by
440 transition layer communities appears unlikely. Our data suggests that sub-surface chlorophyll
441 features can be attributed to photoacclimatation of mixed layer communities within the
442 transition layer, rather than production and subsequent biomass accumulation at this interface.

443 **Late summer transition layers as a site for carbon and silicon decoupling**

444 We propose Southern Ocean transition layers as a key location in the water column
445 where carbon and silicon elemental cycles are decoupled. A notable biogeochemical feature
446 of late summer transition layers in our study region is elevated BSi:POC ratios compared to
447 mixed layer samples (Fig. 4). In contrast to the deep water-column (250 m), mixed layer and
448 transition layer diatom communities are quite similar. This indicates that differences in diatom
449 community structure, (i.e. shifts to larger diatoms in sub-surface communities, Kopczynska et
450 al. 2001) does not act as a major control in driving the patterns in BSi:POC ratios as a
451 function of depth. In contrast, the proportion of empty diatom frustules in the transition layer

452 is markedly increased compared to the mixed layer (Fig. 6). Specifically, we observed an
453 accumulation of empty *F. kerguelensis* and *Pseudo-nitzschia* cells associated to high
454 BSi:POC ratios. Programmed cell death, viral lysis and grazing pressure have all been
455 proposed as mechanisms that could lead to the accumulation of empty frustules (Assmy et al.
456 2013). In this context, transition layers have been identified as grazing hotspots for micro- and
457 meso-zooplankton (Holm-Hansen and Hewes 2004; Gomi et al. 2010). A high BSi:POC ratio
458 is an inherent property to the iron-limited ACC characterized by the dominance of heavily
459 silicified diatoms (Smetacek et al. 2004), our results suggest it might be enhanced within the
460 transition layer transitional layer due to elevated heterotrophic activity and zooplankton
461 grazing. Additionally, transition layers in the SAZ and at A3 displayed a low fraction of
462 empty frustules and a high abundance of large *Corethron* spp. or very large *Thalassiothrix*
463 *antarctica*. The large size of these diatom might confer them a resistance to grazing
464 (Smetacek et al. 2004), resulting in a low proportion of empty frustules for these species.

465 In the AAZ, we observed high $Si(OH)_4$ diffusive fluxes in the transition layer, mainly
466 driven by a strong $Si(OH)_4$ gradient generated by the intense silicon utilization by diatoms in
467 surface waters in summer, and to a lesser extent by an increased Kz within the transition
468 layer. Carbon fixation relies on iron-dependent photosynthesis whereas Si fixation depends on
469 energy from respiration (Martin-Jézéquel et al. 2000) and may thus occur independent of light
470 (Chisholm et al. 1978; Martin-Jézéquel et al. 2000). Silicification may be sustained by vertical
471 diffusion of $Si(OH)_4$ (Table 2) and, even at low levels, may partly contribute to the increase in
472 BSi:POC ratios in AAZ transition layers. Consequently the transition layer may represent a
473 location in the water column where carbon and silicon fixation can become physiologically
474 decoupled, although direct measurements of carbon and silicon uptake (e. g. Closset et al.
475 2014) would be necessary to confirm this hypothesis.

Regional patterns in microplankton diversity and particulate matter stoichiometry

The hierarchical clustering and the CCA suggest strong regional patterns in microplankton community structure relative to the frontal location and the depth. The dominance of the sub-tropical diatom *Bacteriastrum* in the warm surface water waters (15 °C) in the SAZ is likely to result from the southward advection of a the Subtropical Front meander. In general mixed layer communities in the SAZ and PFZ were dominated by the dinoflagellate *Prorocentrum*, in terms of both abundance and biomass. A major contribution of dinoflagellates to late summer phytoplankton biomass was also observed in the SAZ of the Crozet Basin (Kopczyńska and Fiala 2003), although flagellates and coccolithophorids dominated the numerical assemblage (Fiala et al. 2004), consistent with the regional pattern of coccolith sedimentation (Salter et al. 2014). Poulton et al. (2007) reported that post-bloom phytoplankton communities in the PFZ, North of the Crozet plateau, were dominated by the nanoplanktonic *Phaeocystis antarctica*, with a low contribution by the small diatom *Thalassionema nitzschioides*. The low contribution of diatoms to late summer biomass in the mixed layer of the SAZ and PFZ is consistent with the commonly observed succession of diatoms to dinoflagellates from spring to summer (Margalef 1978; Barton et al. 2013). Ciliates significantly contributed to phytoplankton biomass in the mixed layer of the PFZ, indicative of nutrient limitation driving a switch towards a more heterotrophic food-web as often observed at a global scale (Margalef 1958; Landry and Calbet 2004) and during artificial (Gall et al. 2001; Henjes et al. 2007) and natural (Poulton et al. 2007) iron-fertilization studies in the Southern Ocean.

In contrast to the patterns described above, diatoms still heavily dominated AAZ microplankton communities at the time of sampling (>80 % abundance, >70 % biomass), notably through the contribution of large diatoms such as *Membraneis*, *Corethron* and

Rhizosolenia. A dominance of the large diatom *Corethron pennatum* to the total biomass was previoulsy reported in late summer in the AAZ south of Crozet Islands (Poulton et al. 2007). In the AAZ west of South Georgia, diatoms also dominate phytoplankton biomass in late summer with a strong contribution of *Pseudo-nitzschia*, *T. antarctica*, and *E. antarctica* var. *antarctica* (Korb and Whitehouse 2004; Korb et al. 2008, 2010). We observed a strong contribution of the very large diatom *Thalassiothrix antarctica* together with *Corethron* spp. to the total biomass at the central Kerguelen plateau station A3. This is consistent with previous observations at the same station in summer during KEOPS1, although in the latter *E. antarctica* dominated diatom biomass (Armand et al. 2008). On the Kerguelen plateau dinoflagellates contribution to biomass and abundance was lower (mainly though the representation of the genera *Gyrodinium* and *Prorocentrum*) and similar to observations made during KEOPS1 (>20 % microplankton biomass; Sarthou et al. 2008). Over the Kerguelen plateau, diapycnal iron diffusive flux in summer (Blain et al. 2008; Chever et al. 2010) might sustain diatom production and explain why the microplankton community has not shifted to a dominance of dinoflagellates and ciliates.

Regional patterns in PON:POP stoichiometry of particulate matter were strongly correlated with the distribution of major microplankton groups across frontal zones and at different depth horizons. The CCA highlights the general association of elevated PON:POP ratios with dinoflagellates and ciliates. Furthermore, PON:POP ratios were lowest in the mixed layer of the AAZ (4-7) and transition layer of the AAZ (5-8) where biomass is dominated by diatoms (>70 %). In culture, N:P ratios of ~10 for the dinoflagellates *Gymnodinium dominans* and *Oxyrhhis marina* and 10-15 for the ciliate *Euplotes* have been reported (Golz et al. 2015). Under optimal growth conditions *O. marina* exhibits high N:P ratios of 25 (Malzahn et al. 2010). Similarly several studies have reported low N:P ratio from diatom cultures (<10; Quigg et al. 2003; Ho et al. 2003). During the EIFEX artificial-iron

526 fertilization experiment, *F. kerguelensis* was reported to grow with an N:P ratio of 3-4
527 (Hoffmann et al. 2007). During KEOPS2, N:P ratio of 6-15 was found in the high biomass
528 stations of the PFZ east of Kerguelen Islands (Lasbleiz et al. 2014). In agreement with these
529 previous studies, our results suggest that broad-scale shifts in microplankton community
530 composition in the Southern Ocean can modulate particulate matter stoichiometry and are
531 consistent with the major latitudinal trends observed globally (Martiny et al. 2013).

532 There are some notable subtleties to the general trends presented above. SAZ mixed
533 layer particles exhibit relatively high PON:POP ratios (10-12) even if the community was
534 dominated by diatoms (e.g. Station 5; >75% *Bacteriastrum* sp.). Resource allocation in
535 Southern Ocean diatoms is known to be highly sensitive to temperature with more P-rich
536 ribosomes being required for protein synthesis under low temperature resulting in a lower N:P
537 ratio (Toseland et al. 2013). Mixed layer waters of the SAZ are notably warmer (10-15°C)
538 than the AAZ (2-4°C), which may result in higher PON:POP ratio for diatom-dominated
539 communities of the SAZ compared to the AAZ. Iron-limitation is an additional plausible
540 mechanism that may modulate PON:POP ratios. Iron limitation decreases nitrate uptake
541 (Price et al. 1994) and nitrate reductase activity (Timmermans et al. 1994), leading to lower
542 N:P ratio in iron-limited diatom cultures (Price 2005). Furthermore, Hoffmann et al. (2006)
543 reported a strong N:P increase (4 to 16) in the >20 µm fraction following iron addition in
544 iron-limited cultures. The dissolved iron concentration is <0.15 nmol L^{-1} in the mixed layer in
545 the AAZ over the central Kerguelen plateau in February (Blain et al. 2008) and therefore iron
546 limitation may have lowered PON:POP ratios observed in the diatom-dominated AAZ
547 samples. In conclusion microplankton community structure appears to exert a first order
548 control on PON:POP stoichiometry in late summer in this sector of the Southern Ocean.
549 Physiological constraints linked to environmental factors, such as temperature and iron
550 limitation, are also able to modulate this ratio.

551 **Implications for carbon and silicon export**

552 A recent compilation of carbon export estimates over the Kerguelen plateau (station A3)
553 indicates a strong POC flux attenuation between the mixed layer and 300 m (Rembauville et
554 al. 2015b). In this region we observed similarly high BSi:POC ratios in the transition layer
555 (~0.8) compared to sediment trap samples (0.7 – 1.5) at the end of summer (Rembauville et
556 al. 2015a). *F. kerguelensis* was mostly present in the form of empty frustules in the transition
557 layer, consistent with its classification as a preferential "silica sinker" (Assmy et al. 2013;
558 Smetacek et al. 2004) that has been confirmed by sediment trap studies (Salter et al. 2012;
559 Rembauville et al. 2015a; Rigual-Hernández et al. 2015). In contrast, the large *Rhizosolenia*
560 spp. (~500 µm) and very large *T. antarctica* (up to 3-4 mm) were present as full cells within
561 the transition layer, an observation consistent with their recent quantification as a "carbon
562 sinker" over the central Kerguelen plateau (Rembauville et al. 2015a). However, the large
563 frustule of these species confers a resistance to grazing (e.g. Smetacek et al. 2004) and high
564 Si:C ratio that may drive a significant contribution to silicon sinking.

565 It is generally stated that diatom-dominated ecosystems are more efficient in exporting
566 carbon from the mixed layer compared to more recycling systems dominated by
567 dinoflagellates and ciliates (Smetacek 1985; Legendre and le Fèvre 1989; Boyd and Newton
568 1995, 1999; Legendre and Rivkin 2015). However, despite a dominance of diatoms in the
569 mixed layer microplankton assemblage in the AAZ, the deep (250 m) POC concentrations in
570 the AAZ were comparable to the PFZ and SAZ (0.9-1.36 µmol L^{-1} versus 1.10 – 1.90 µmol L^{-1})
571 where dinoflagelates and ciliates dominated the microplankton assemblage. Although one
572 must be cautious in equating standing stocks to fluxes these data suggest that in late summer
573 in the Southern Ocean, a higher proportion of diatoms in the mixed layer does not consistently
574 lead to a higher transfer of carbon at 250 m. Intense zooplankton grazing of diatom biomass in
575 the transition layer, as evidenced by the increased proportion of empty cells relative to the

mixed layer, presumably results in the efficient consumption and recycling of exportable biomass reducing diatom-mediated carbon transfer into the ocean interior. This has been suggested previously as an explanation for High biomass Low Export Environments (Lam and Bishop 2007; Lam et al. 2011; Jacquet et al. 2011). Moreover, a strong response of heterotrophic microbial communities to the high primary production levels (Obernosterer et al. 2008) and the association of specific bacterial communities with deep biomass features (Obernosterer et al. 2011) might also strongly contribute to the remineralization of POC over the Kerguelen plateau. An efficient response of both microbial and mesozooplanktonic communities to POC availability is consistent with the inverse relationship between diatom-dominated primary production and export efficiency observed in the Southern Ocean (Maiti et al. 2013). Furthermore we observed a progressive increase of diatoms present as empty frustules through the water column and a significantly higher contribution of dinoflagellates and ciliates to total microplankton POC at 250 m compared to the transition layer. These data show the importance of zooplankton grazing in modulating diatom export production during late summer Southern Ocean ecosystems and highlight the potential importance of ciliates and dinoflagellates to the biological carbon pump at these specific times.

A notable exception to the patterns described above are the observations from station A3, on the Kerguelen plateau, where deep microplankton POC is dominated by *Chaetoceros* Hyalocahete resting spores (80%), leading to POC concentrations that are ~3 times higher than mean values at 250 m in the AAZ, PFZ and SAZ. This observation is broadly consistent with a recent sediment trap study which documented *C. Hyalochaete* resting spores as the dominant contributor to the annual carbon (>60%) mediated through two rapid flux events occurring at the end of summer (Rembauville et al. 2015a). If the transition layer is a place of intense grazing pressure then our results consolidate the idea that resting spores are a specific ecological vector for carbon export through intense remineralization horizons. Indeed, small

and highly silicified *Chaetoceros Hyalochaete* resting spores have been demonstrated to lower copepod grazing pressure in culture (Kuwata and Tsuda 2005). In line with recent sediment trap results, the present study supports the pivotal role of diatom resting spores for carbon export from natural iron fertilized blooms in the Southern Ocean (Salter et al. 2007, 2012; Rembauville et al. 2015a). The net impact of diatom-dominated communities on carbon export strongly depends on the ecology of the species present. Preferential silicon sinking species poorly contribute to carbon export contrary to carbon sinking species, such as diatoms that form resting spores. A coupled description of mixed layer properties (nutrient dynamics and phytoplankton communities) and export out of the mixed layer over an entire productive cycle remains necessary to better understand processes responsible for resting spore formation.

References

Aminot, A., and R. Kerouel. 2007. Dosage automatique des nutriments dans les eaux marines: méthodes en flux continu, Ifremer.

Anning, T., H. L. MacIntyre, S. M. Pratt, P. J. Sammes, S. Gibb, and R. J. Geider. 2000. Photoacclimation in the marine diatom *Skeletonema costatum*. Limnol. Oceanogr. **45**: 1807–1817. doi:10.4319/lo.2000.45.8.1807

Armand, L. K., V. Cornet-Barthaux, J. Mosseri, and B. Quéguiner. 2008. Late summer diatom biomass and community structure on and around the naturally iron-fertilised Kerguelen Plateau in the Southern Ocean. Deep Sea Res. Part II Top. Stud. Oceanogr. **55**: 653–676. doi:10.1016/j.dsr2.2007.12.031

Assmy, P., V. Smetacek, M. Montresor, and others. 2013. Thick-shelled, grazer-protected diatoms decouple ocean carbon and silicon cycles in the iron-limited Antarctic Circumpolar Current. Proc. Natl. Acad. Sci. **110**: 20633–20638. doi:10.1073/pnas.1309345110

de Baar, H. J. W., A. G. J. Buma, R. F. Nolting, G. C. Cadée, G. Jacques, and P. Tréguer. 1990. On iron limitation of the Southern Ocean: experimental observations in the Weddell and Scotia Seas. Mar. Ecol. Prog. Ser. **65**: 105–122. doi:10.3354/meps065105

Barton, A. D., Z. V. Finkel, B. A. Ward, D. G. Johns, and M. J. Follows. 2013. On the roles of cell size and trophic strategy in North Atlantic diatom and dinoflagellate communities. Limnol. Oceanogr. **58**: 254–266. doi:10.4319/lo.2013.58.1.0254

Blain, S., G. Sarthou, and P. Laan. 2008. Distribution of dissolved iron during the natural iron-fertilization experiment KEOPS (Kerguelen Plateau, Southern Ocean). Deep Sea Res. Part II Top. Stud. Oceanogr. **55**: 594–605. doi:10.1016/j.dsr2.2007.12.028

637 Blain, S., P. Tréguer, S. Belviso, and others. 2001. A biogeochemical study of the island mass
638 effect in the context of the iron hypothesis: Kerguelen Islands, Southern Ocean. Deep
639 Sea Res. Part I Oceanogr. Res. Pap. **48**: 163–187. doi:10.1016/S0967-0637(00)00047-
640 9
641 Borrione, I., and R. Schlitzer. 2013. Distribution and recurrence of phytoplankton blooms
642 around South Georgia, Southern Ocean. Biogeosciences **10**: 217–231. doi:10.5194/bg-
643 10-217-2013
644 Boyd, P., and P. Newton. 1995. Evidence of the potential influence of planktonic community
645 structure on the interannual variability of particulate organic carbon flux. Deep Sea
646 Res. Part I Oceanogr. Res. Pap. **42**: 619–639. doi:10.1016/0967-0637(95)00017-Z
647 Boyd, P. W., and P. P. Newton. 1999. Does planktonic community structure determine
648 downward particulate organic carbon flux in different oceanic provinces? Deep Sea
649 Res. Part I Oceanogr. Res. Pap. **46**: 63–91. doi:10.1016/S0967-0637(98)00066-1
650 de Boyer Montégut, C., G. Madec, A. S. Fischer, A. Lazar, and D. Iudicone. 2004. Mixed
651 layer depth over the global ocean: An examination of profile data and a profile-based
652 climatology. J. Geophys. Res. Oceans **109**: C12003. doi:10.1029/2004JC002378
653 Chever, F., G. Sarthou, E. Bucciarelli, S. Blain, and A. R. Bowie. 2010. An iron budget
654 during the natural iron fertilisation experiment KEOPS (Kerguelen Islands, Southern
655 Ocean). Biogeosciences **7**: 455–468. doi:10.5194/bg-7-455-2010
656 Chisholm, S. W., F. Azam, and R. W. Eppley. 1978. Silicic acid incorporation in marine
657 diatoms on light:dark cycles: Use as an assay for phased cell division 1. Limnol.
658 Oceanogr. **23**: 518–529. doi:10.4319/lo.1978.23.3.0518
659 Cloern, J. E., C. Grenz, and L. Vidergar-Lucas. 1995. An empirical model of the
660 phytoplankton chlorophyll : carbon ratio-the conversion factor between productivity
661 and growth rate. Limnol. Oceanogr. **40**: 1313–1321. doi:10.4319/lo.1995.40.7.1313

662 Closset, I., M. Lasbleiz, K. Leblanc, B. Quéguiner, A.-J. Cavagna, M. Elskens, J. Navez, and
663 D. Cardinal. 2014. Seasonal evolution of net and regenerated silica production around
664 a natural Fe-fertilized area in the Southern Ocean estimated with Si isotopic
665 approaches. Biogeosciences **11**: 5827–5846. doi:10.5194/bg-11-5827-2014
666 Cornet-Barthaux, V., L. Armand, and B. Quéguiner. 2007. Biovolume and biomass estimates
667 of key diatoms in the Southern Ocean. Aquat. Microb. Ecol. **48**: 295–308.
668 doi:10.3354/ame048295
669 Dutkiewicz, S., M. J. Follows, and P. Parekh. 2005. Interactions of the iron and phosphorus
670 cycles: A three-dimensional model study. Glob. Biogeochem. Cycles **19**: GB1021.
671 doi:10.1029/2004GB002342
672 Elser, J. J., D. R. Dobberfuhl, N. A. MacKay, and J. H. Schampel. 1996. Organism Size, Life
673 History, and N:P Stoichiometry. BioScience **46**: 674–684. doi:10.2307/1312897
674 Fennel, K., and E. Boss. 2003. Subsurface maxima of phytoplankton and chlorophyll: Steady-
675 state solutions from a simple model. Limnol. Oceanogr. **48**: 1521–1534.
676 doi:10.4319/lo.2003.48.4.1521
677 Fiala, M., E. E. Kopczynska, L. Oriol, and M.-C. Machado. 2004. Phytoplankton variability in
678 the Crozet Basin frontal zone (Southwest Indian Ocean) during austral summer. J.
679 Mar. Syst. **50**: 243–261. doi:10.1016/j.jmarsys.2004.01.008
680 Gall, M. P., P. W. Boyd, J. Hall, K. A. Safi, and H. Chang. 2001. Phytoplankton processes.
681 Part 1: Community structure during the Southern Ocean Iron RElease Experiment
682 (SOIREE). Deep Sea Res. Part II Top. Stud. Oceanogr. **48**: 2551–2570.
683 doi:10.1016/S0967-0645(01)00008-X
684 Golz, A.-L., A. Burian, and M. Winder. 2015. Stoichiometric regulation in micro- and
685 mesozooplankton. J. Plankton Res. **37**: 293–305. doi:10.1093/plankt/fbu109

686 Gomi, Y., M. Fukuchi, and A. Taniguchi. 2010. Diatom assemblages at subsurface
687 chlorophyll maximum layer in the eastern Indian sector of the Southern Ocean in
688 summer. J. Plankton Res. **32**: 1039–1050. doi:10.1093/plankt/fbq031
689 Gordon, H. R., and W. R. McCluney. 1975. Estimation of the depth of sunlight penetration in
690 the sea for remote sensing. Appl. Opt. **14**: 413–416.
691 Hasle, G. R., and E. E. Syvertsen. 1997. Chapter 2 - Marine Diatoms, p. 5–385. *In* C.R.
692 Tomas [ed.], Identifying Marine Phytoplankton. Academic Press.
693 Henjes, J., P. Assmy, C. Klaas, P. Verity, and V. Smetacek. 2007. Response of
694 microzooplankton (protists and small copepods) to an iron-induced phytoplankton
695 bloom in the Southern Ocean (EisenEx). Deep Sea Res. Part I Oceanogr. Res. Pap. **54**:
696 363–384. doi:10.1016/j.dsr.2006.12.004
697 Hillebrand, H., C.-D. Dürselen, D. Kirschtel, U. Pollingher, and T. Zohary. 1999. Biovolume
698 Calculation for Pelagic and Benthic Microalgae. J. Phycol. **35**: 403–424.
699 doi:10.1046/j.1529-8817.1999.3520403.x
700 Hoffmann, L. J., I. Peeken, and K. Lochte. 2007. Effects of iron on the elemental
701 stoichiometry during EIFEX and in the diatoms Fragilariopsis kerguelensis and
702 Chaetoceros dichaeta. Biogeosciences **4**: 569–579. doi:10.5194/bg-4-569-2007
703 Hoffmann, L. J., I. Peeken, K. Lochte, P. Assmy, and M. Veldhuis. 2006. Different reactions
704 of Southern Ocean phytoplankton size classes to iron fertilization. Limnol. Oceanogr.
705 **51**: 1217–1229. doi:10.4319/lo.2006.51.3.1217
706 Holm-Hansen, O., and C. D. Hewes. 2004. Deep chlorophyll-a maxima (DCMs) in Antarctic
707 waters. I. Relationships between DCMs and the physical, chemical, and optical
708 conditions in the upper water column. Polar Biol. **27**: 699–710. doi:10.1007/s00300-
709 004-0641-1

Holm-Hansen, O., M. Kahru, and C. Hewes. 2005. Deep chlorophyll a maxima (DCMs) in pelagic Antarctic waters. II. Relation to bathymetric features and dissolved iron concentrations. Mar. Ecol. Prog. Ser. **297**: 71–81. doi:10.3354/meps297071

Ho, T.-Y., A. Quigg, Z. V. Finkel, A. J. Milligan, K. Wyman, P. G. Falkowski, and F. M. M. Morel. 2003. The Elemental Composition of Some Marine Phytoplankton. J. Phycol. **39**: 1145–1159. doi:10.1111/j.0022-3646.2003.03-090.x

Howard, A. G., A. J. Coxhead, I. A. Potter, and A. P. Watt. 1986. Determination of dissolved aluminium by the micelle-enhanced fluorescence of its lumogallion complex. Analyst **111**: 1379–1382. doi:10.1039/AN9861101379

Hutchins, D. A., and K. W. Bruland. 1998. Iron-limited diatom growth and Si:N uptake ratios in a coastal upwelling regime. Nature **393**: 561–564. doi:10.1038/31203

Jacquet, S. H. ., P. J. Lam, T. Trull, and F. Dehairs. 2011. Carbon export production in the subantarctic zone and polar front zone south of Tasmania. Deep Sea Res. Part II Top. Stud. Oceanogr. **58**: 2277–2292. doi:10.1016/j.dsr2.2011.05.035

Johnston, T. M. S., and D. L. Rudnick. 2009. Observations of the Transition Layer. J. Phys. Oceanogr. **39**: 780–797. doi:10.1175/2008JPO3824.1

Khatiwala, S., F. Primeau, and T. Hall. 2009. Reconstruction of the history of anthropogenic CO_2 concentrations in the ocean. Nature **462**: 346–349. doi:10.1038/nature08526

Klausmeier, C. A., E. Litchman, T. Daufresne, and S. A. Levin. 2004. Optimal nitrogen-to-phosphorus stoichiometry of phytoplankton. Nature **429**: 171–174. doi:10.1038/nature02454

Kopczynska, E. E., F. Dehairs, M. Elskens, and S. Wright. 2001. Phytoplankton and microzooplankton variability between the Subtropical and Polar Fronts south of Australia: Thriving under regenerative and new production in late summer. J. Geophys. Res. Oceans **106**: 31597–31609. doi:10.1029/2000JC000278

735 Kopczyńska, E. E., and M. Fiala. 2003. Surface phytoplankton composition and carbon
736 biomass distribution in the Crozet Basin during austral summer of 1999: variability
737 across frontal zones. Polar Biol. **27**: 17–28. doi:10.1007/s00300-003-0564-2
738 Korb, R. E., and M. Whitehouse. 2004. Contrasting primary production regimes around South
739 Georgia, Southern Ocean: large blooms versus high nutrient, low chlorophyll waters.
740 Deep Sea Res. Part I Oceanogr. Res. Pap. **51**: 721–738. doi:10.1016/j.dsr.2004.02.006
741 Korb, R. E., M. J. Whitehouse, A. Atkinson, and S. E. Thorpe. 2008. Magnitude and
742 maintenance of the phytoplankton bloom at South Georgia: a naturally iron-replete
743 environment. Mar. Ecol. Prog. Ser. **368**: 75–91. doi:10.3354/meps07525
744 Korb, R. E., M. J. Whitehouse, M. Gordon, P. Ward, and A. J. Poulton. 2010. Summer
745 microplankton community structure across the Scotia Sea: implications for biological
746 carbon export. Biogeosciences **7**: 343–356. doi:10.5194/bg-7-343-2010
747 Kuwata, A., and A. Tsuda. 2005. Selection and viability after ingestion of vegetative cells,
748 resting spores and resting cells of the marine diatom, Chaetoceros pseudocurvisetus,
749 by two copepods. J. Exp. Mar. Biol. Ecol. **322**: 143–151.
750 doi:10.1016/j.jembe.2005.02.013
751 Lam, P. J., and J. K. B. Bishop. 2007. High biomass, low export regimes in the Southern
752 Ocean. Deep Sea Res. Part II Top. Stud. Oceanogr. **54**: 601–638.
753 doi:10.1016/j.dsr2.2007.01.013
754 Lam, P. J., S. C. Doney, and J. K. B. Bishop. 2011. The dynamic ocean biological pump:
755 Insights from a global compilation of particulate organic carbon, CaCO3, and opal
756 concentration profiles from the mesopelagic. Glob. Biogeochem. Cycles **25**: GB3009.
757 doi:10.1029/2010GB003868
758 Landry, M. R., and A. Calbet. 2004. Microzooplankton production in the oceans. ICES J.
759 Mar. Sci. J. Cons. **61**: 501–507. doi:10.1016/j.icesjms.2004.03.011

760 Lasbleiz, M., K. Leblanc, S. Blain, J. Ras, V. Cornet-Barthaux, S. Hélias Nunige, and B.
761 Quéguiner. 2014. Pigments, elemental composition (C, N, P, and Si), and
762 stoichiometry of particulate matter in the naturally iron fertilized region of Kerguelen
763 in the Southern Ocean. Biogeosciences **11**: 5931–5955. doi:10.5194/bg-11-5931-2014
764 Legendre, L., and J. le Fèvre. 1989. Hydrodynamical singularities as controls of recycled
765 versus export production in oceans, p. 49–63. *In* Productivity of the oceans: present
766 and past. Berger, W. H., Smetacek, V. S., Wefer, G.
767 Legendre, L., and R. B. Rivkin. 2015. Flows of biogenic carbon within marine pelagic food
768 webs: roles of microbial competition switches. Mar. Ecol. Prog. Ser. **521**: 19–30.
769 doi:10.3354/meps11124
770 Legendre, P., and L. Legendre. 1998. Numerical Ecology, Édition : 2. Elsevier Science.
771 Letelier, R. M., D. M. Karl, M. R. Abbott, and R. R. Bidigare. 2004. Light driven seasonal
772 patterns of chlorophyll and nitrate in the lower euphotic zone of the North Pacific
773 Subtropical Gyre. Limnol. Oceanogr. **49**: 508–519. doi:10.4319/lo.2004.49.2.0508
774 Maiti, K., M. A. Charette, K. O. Buesseler, and M. Kahru. 2013. An inverse relationship
775 between production and export efficiency in the Southern Ocean. Geophys. Res. Lett.
776 **40**: 1557–1561. doi:10.1002/grl.50219
777 Malzahn, A. M., F. Hantzsche, K. L. Schoo, M. Boersma, and N. Aberle. 2010. Differential
778 effects of nutrient-limited primary production on primary, secondary or tertiary
779 consumers. Oecologia **162**: 35–48. doi:10.1007/s00442-009-1458-y
780 Margalef, R. 1958. Temporal succession and spatial heterogeneity in phytoplankton., p. 323–
781 349. *In* Perspective in marine biology. Buzzat-Traverso, A. A.
782 Margalef, R. 1978. Life-forms of phytoplankton as survival alternatives in an unstable
783 environment. Oceanol. Acta **1**: 493–509.

784 Martin-Jézéquel, V., M. Hildebrand, and M. A. Brzezinski. 2000. Silicon Metabolism in
785 Diatoms: Implications for Growth. J. Phycol. **36**: 821–840. doi:10.1046/j.1529-
786 8817.2000.00019.x
787 Martin, J. H. 1990. Glacial-interglacial CO_2 change: The Iron Hypothesis. Paleoceanography
788 **5**: 1–13. doi:10.1029/PA005i001p00001
789 Martin, J., J. Tremblay, J. Gagnon, and others. 2010. Prevalence, structure and properties of
790 subsurface chlorophyll maxima in Canadian Arctic waters. Mar. Ecol. Prog. Ser. **412**:
791 69–84. doi:10.3354/meps08666
792 Martiny, A. C., C. T. A. Pham, F. W. Primeau, J. A. Vrugt, J. K. Moore, S. A. Levin, and M.
793 W. Lomas. 2013. Strong latitudinal patterns in the elemental ratios of marine plankton
794 and organic matter. Nat. Geosci. **6**: 279–283. doi:10.1038/ngeo1757
795 Menden-Deuer, S., and E. J. Lessard. 2000. Carbon to volume relationships for
796 dinoflagellates, diatoms, and other protist plankton. Limnol. Oceanogr. **45**: 569–579.
797 doi:10.4319/lo.2000.45.3.0569
798 Mignot, A., H. Claustre, J. Uitz, A. Poteau, F. D'Ortenzio, and X. Xing. 2014. Understanding
799 the seasonal dynamics of phytoplankton biomass and the deep chlorophyll maximum
800 in oligotrophic environments: A Bio-Argo float investigation. Glob. Biogeochem.
801 Cycles **28**: 2013GB004781. doi:10.1002/2013GB004781
802 Minas, H. J., M. Minas, and T. T. Packard. 1986. Productivity in upwelling areas deduced
803 from hydrographic and chemical fields. Limnol. Oceanogr. **31**: 1182–1206.
804 doi:10.4319/lo.1986.31.6.1182
805 Moore, C. M., A. E. Hickman, A. J. Poulton, S. Seeyave, and M. I. Lucas. 2007. Iron–light
806 interactions during the CROZet natural iron bloom and EXport experiment
807 (CROZEX): II—Taxonomic responses and elemental stoichiometry. Deep Sea Res.
808 Part II Top. Stud. Oceanogr. **54**: 2066–2084. doi:10.1016/j.dsr2.2007.06.015

809 Morel, A., and J.-F. Berthon. 1989. Surface pigments, algal biomass profiles, and potential
810 production of the euphotic layer: Relationships reinvestigated in view of remote-
811 sensing applications. Limnol. Oceanogr. **34**: 1545–1562.
812 doi:10.4319/lo.1989.34.8.1545
813 Mosseri, J., B. Quéguiner, L. Armand, and V. Cornet-Barthaux. 2008. Impact of iron on
814 silicon utilization by diatoms in the Southern Ocean: A case study of Si/N cycle
815 decoupling in a naturally iron-enriched area. Deep Sea Res. Part II Top. Stud.
816 Oceanogr. **55**: 801–819. doi:10.1016/j.dsr2.2007.12.003
817 Neveux, J., and F. Lantoine. 1993. Spectrofluorometric assay of chlorophylls and
818 phaeopigments using the least squares approximation technique. Deep Sea Res. Part I
819 Oceanogr. Res. Pap. **40**: 1747–1765. doi:10.1016/0967-0637(93)90030-7
820 Obernosterer, I., P. Catala, P. Lebaron, and N. J. West. 2011. Distinct bacterial groups
821 contribute to carbon cycling during a naturally iron fertilized phytoplankton bloom in
822 the Southern Ocean. Limnol. Oceanogr. **56**: 2391–2401.
823 doi:10.4319/lo.2011.56.6.2391
824 Obernosterer, I., U. Christaki, D. Lefèvre, P. Catala, F. Van Wambeke, and P. Lebaron. 2008.
825 Rapid bacterial mineralization of organic carbon produced during a phytoplankton
826 bloom induced by natural iron fertilization in the Southern Ocean. Deep Sea Res. Part
827 II Top. Stud. Oceanogr. **55**: 777–789. doi:10.1016/j.dsr2.2007.12.005
828 Park, J., I.-S. Oh, H.-C. Kim, and S. Yoo. 2010. Variability of SeaWiFs chlorophyll-a in the
829 southwest Atlantic sector of the Southern Ocean: Strong topographic effects and weak
830 seasonality. Deep Sea Res. Part I Oceanogr. Res. Pap. **57**: 604–620.
831 doi:10.1016/j.dsr.2010.01.004
832 Park, Y.-H., E. Charriaud, D. R. Pino, and C. Jeandel. 1998. Seasonal and interannual
833 variability of the mixed layer properties and steric height at station KERFIX,

834 southwest of Kerguelen. J. Mar. Syst. **17**: 571–586. doi:10.1016/S0924-
835 7963(98)00065-7
836 Park, Y.-H., J.-H. Lee, I. Durand, and C.-S. Hong. 2014. Validation of Thorpe-scale-derived
837 vertical diffusivities against microstructure measurements in the Kerguelen region.
838 Biogeosciences **11**: 6927–6937. doi:10.5194/bg-11-6927-2014
839 Parslow, J. S., P. W. Boyd, S. R. Rintoul, and F. B. Griffiths. 2001. A persistent subsurface
840 chlorophyll maximum in the Interpolar Frontal Zone south of Australia: Seasonal
841 progression and implications for phytoplankton-light-nutrient interactions. J. Geophys.
842 Res. Oceans **106**: 31543–31557. doi:10.1029/2000JC000322
843 Pollard, R. T., H. J. Venables, J. F. Read, and J. T. Allen. 2007. Large-scale circulation
844 around the Crozet Plateau controls an annual phytoplankton bloom in the Crozet
845 Basin. Deep Sea Res. Part II Top. Stud. Oceanogr. **54**: 1915–1929.
846 doi:10.1016/j.dsr2.2007.06.012
847 Poulton, A. J., C. Mark Moore, S. Seeyave, M. I. Lucas, S. Fielding, and P. Ward. 2007.
848 Phytoplankton community composition around the Crozet Plateau, with emphasis on
849 diatoms and Phaeocystis. Deep Sea Res. Part II Top. Stud. Oceanogr. **54**: 2085–2105.
850 doi:10.1016/j.dsr2.2007.06.005
851 Price, N. M. 2005. The elemental stoichiometry and composition of an iron-limited diatom.
852 Limnol. Oceanogr. **50**: 1159–1171. doi:10.4319/lo.2005.50.4.1159
853 Price, N. M., B. A. Ahner, and F. M. M. Morel. 1994. The Equatorial Pacific Ocean: Grazer-
854 Controlled Phytoplankton Populations in an Iron-Limited Ecosystem. Limnol.
855 Oceanogr. **39**: 520–534.
856 Primeau, F. W., M. Holzer, and T. DeVries. 2013. Southern Ocean nutrient trapping and the
857 efficiency of the biological pump. J. Geophys. Res. Oceans **118**: 2547–2564.
858 doi:10.1002/jgrc.20181

Pujo-Pay, M., and P. Raimbault. 1994. Improvement of the wet-oxidation procedure for simultaneous determination of particulate organic nitrogen and phosphorus collected on filters. Mar. Ecol. Prog. Ser. **105**: 203–207.

Quéguiner, B. 2013. Iron fertilization and the structure of planktonic communities in high nutrient regions of the Southern Ocean. Deep Sea Res. Part II Top. Stud. Oceanogr. **90**: 43–54. doi:10.1016/j.dsr2.2012.07.024

Quéguiner, B., and M. A. Brzezinski. 2002. Biogenic silica production rates and particulate organic matter distribution in the Atlantic sector of the Southern Ocean during austral spring 1992. Deep Sea Res. Part II Top. Stud. Oceanogr. **49**: 1765–1786. doi:10.1016/S0967-0645(02)00011-5

Quigg, A., Z. V. Finkel, A. J. Irwin, and others. 2003. The evolutionary inheritance of elemental stoichiometry in marine phytoplankton. Nature **425**: 291–294. doi:10.1038/nature01953

Ragueneau, O., N. Savoye, Y. Del Amo, J. Cotten, B. Tardiveau, and A. Leynaert. 2005. A new method for the measurement of biogenic silica in suspended matter of coastal waters: using Si:Al ratios to correct for the mineral interference. Cont. Shelf Res. **25**: 697–710. doi:10.1016/j.csr.2004.09.017

Redfield, A. C. 1958. The biological control of chemical factors in the environment. Am Sc **11**: 205–221.

Rembauville, M., S. Blain, L. Armand, B. Quéguiner, and I. Salter. 2015a. Export fluxes in a naturally iron-fertilized area of the Southern Ocean – Part 2: Importance of diatom resting spores and faecal pellets for export. Biogeosciences **12**: 3171–3195. doi:10.5194/bg-12-3171-2015

Rembauville, M., I. Salter, N. Leblond, A. Gueneugues, and S. Blain. 2015b. Export fluxes in a naturally iron-fertilized area of the Southern Ocean – Part 1: Seasonal dynamics of

884 particulate organic carbon export from a moored sediment trap. Biogeosciences **12**:
885 3153–3170. doi:10.5194/bg-12-3153-2015
886 Rigual-Hernández, A. S., T. W. Trull, S. G. Bray, A. Cortina, and L. K. Armand. 2015.
887 Latitudinal and temporal distributions of diatom populations in the pelagic waters of
888 the Subantarctic and Polar Frontal zones of the Southern Ocean and their role in the
889 biological pump. Biogeosciences **12**: 5309–5337. doi:10.5194/bg-12-5309-2015
890 Sabine, C. L., R. A. Feely, N. Gruber, and others. 2004. The Oceanic Sink for Anthropogenic
891 CO_2. Science **305**: 367–371. doi:10.1126/science.1097403
892 Salter, I., A. E. S. Kemp, C. M. Moore, R. S. Lampitt, G. A. Wolff, and J. Holtvoeth. 2012.
893 Diatom resting spore ecology drives enhanced carbon export from a naturally iron-
894 fertilized bloom in the Southern Ocean. Glob. Biogeochem. Cycles **26**: GB1014.
895 doi:10.1029/2010GB003977
896 Salter, I., R. S. Lampitt, R. Sanders, A. Poulton, A. E. S. Kemp, B. Boorman, K. Saw, and R.
897 Pearce. 2007. Estimating carbon, silica and diatom export from a naturally fertilised
898 phytoplankton bloom in the Southern Ocean using PELAGRA: A novel drifting
899 sediment trap. Deep Sea Res. Part II Top. Stud. Oceanogr. **54**: 2233–2259.
900 doi:10.1016/j.dsr2.2007.06.008
901 Salter, I., R. Schiebel, P. Ziveri, A. Movellan, R. Lampitt, and G. A. Wolff. 2014. Carbonate
902 counter pump stimulated by natural iron fertilization in the Polar Frontal Zone. Nat.
903 Geosci. **7**: 885–889. doi:10.1038/ngeo2285
904 Sarmiento, J. L., N. Gruber, M. A. Brzezinski, and J. P. Dunne. 2004. High-latitude controls
905 of thermocline nutrients and low latitude biological productivity. Nature **427**: 56–60.
906 doi:10.1038/nature02127

907 Sarthou, G., K. R. Timmermans, S. Blain, and P. Tréguer. 2005. Growth physiology and fate
908 of diatoms in the ocean: a review. J. Sea Res. **53**: 25–42.
909 doi:10.1016/j.seares.2004.01.007
910 Sarthou, G., D. Vincent, U. Christaki, I. Obernosterer, K. R. Timmermans, and C. P. D.
911 Brussaard. 2008. The fate of biogenic iron during a phytoplankton bloom induced by
912 natural fertilisation: Impact of copepod grazing. Deep Sea Res. Part II Top. Stud.
913 Oceanogr. **55**: 734–751. doi:10.1016/j.dsr2.2007.12.033
914 Shih, L. H., J. R. Koseff, G. N. Ivey, and J. H. Ferziger. 2005. Parameterization of turbulent
915 fluxes and scales using homogeneous sheared stably stratified turbulence simulations.
916 J. Fluid Mech. **525**: 193–214. doi:10.1017/S0022112004002587
917 Smetacek, V., P. Assmy, and J. Henjes. 2004. The role of grazing in structuring Southern
918 Ocean pelagic ecosystems and biogeochemical cycles. Antarct. Sci. **16**: 541–558.
919 doi:10.1017/S0954102004002317
920 Smetacek, V. S. 1985. Role of sinking in diatom life-history cycles: ecological, evolutionary
921 and geological significance. Mar. Biol. **84**: 239–251. doi:10.1007/BF00392493
922 Sterner, R. W., and J. J. Elser. 2002. Ecological Stoichiometry: The Biology of Elements from
923 Molecules to the Biosphere, Princeton University Press.
924 Strzepek, R. F., K. A. Hunter, R. D. Frew, P. J. Harrison, and P. W. Boyd. 2012. Iron-light
925 interactions differ in Southern Ocean phytoplankton. Limnol. Oceanogr. **57**: 1182–
926 1200. doi:10.4319/lo.2012.57.4.1182
927 Tagliabue, A., J.-B. Sallée, A. R. Bowie, M. Lévy, S. Swart, and P. W. Boyd. 2014. Surface-
928 water iron supplies in the Southern Ocean sustained by deep winter mixing. Nat.
929 Geosci. **7**: 314–320. doi:10.1038/ngeo2101
930 Takeda, S. 1998. Influence of iron availability on nutrient consumption ratio of diatoms in
931 oceanic waters. Nature **393**: 774–777. doi:10.1038/31674

Timmermans, K. R., W. Stolte, and H. J. W. de Baar. 1994. Iron-mediated effects on nitrate reductase in marine phytoplankton. Mar. Biol. **121**: 389–396. doi:10.1007/BF00346749

Toseland, A., S. J. Daines, J. R. Clark, and others. 2013. The impact of temperature on marine phytoplankton resource allocation and metabolism. Nat. Clim. Change **3**: 979–984. doi:10.1038/nclimate1989

Uitz, J., H. Claustre, F. B. Griffiths, J. Ras, N. Garcia, and V. Sandroni. 2009. A phytoplankton class-specific primary production model applied to the Kerguelen Islands region (Southern Ocean). Deep Sea Res. Part I Oceanogr. Res. Pap. **56**: 541–560. doi:10.1016/j.dsr.2008.11.006

Van Mooy, B. A. S., H. F. Fredricks, B. E. Pedler, and others. 2009. Phytoplankton in the ocean use non-phosphorus lipids in response to phosphorus scarcity. Nature **458**: 69–72. doi:10.1038/nature07659

Venrick, E. L., J. A. McGowan, and A. W. Mantyla. 1973. Deep maxima of photosynthetic chlorophyll in Pacific Ocean. Fish. Bull. **71**: 41–52.

Weber, T. S., and C. Deutsch. 2010. Ocean nutrient ratios governed by plankton biogeography. Nature **467**: 550–554. doi:10.1038/nature09403

Weston, K., L. Fernand, D. K. Mills, R. Delahunty, and J. Brown. 2005. Primary production in the deep chlorophyll maximum of the central North Sea. J. Plankton Res. **27**: 909–922. doi:10.1093/plankt/fbi064

Whitehouse, M. J., J. Priddle, and M. A. Brandon. 2000. Chlorophyll/nutrient characteristics in the water masses to the north of South Georgia, Southern Ocean. Polar Biol. **23**: 373–382. doi:10.1007/s003000050458

Acknowledgements.

We thank the captain Bernard Lassiette and crew of the R/V Marion Dufresne for their support aboard as well as the chief scientist Yves Cherel. We thank Claire Lo Monaco and Céline Ridame for the access to the CTD and chlorophyll a data and Isabelle Durand for the help in the Thorpe displacement calculation. We thank the three anonymous reviewers for their constructive comments, which helped us to improve the manuscript. This work was supported by grants from the French research program of INSU-CNRS LEFE-CYBER (EXPLAIN, Ian Salter) and the French ANR (KEOPS2, ANR-10-BLAN-0614, Stéphane Blain). The OISO program is supported by the French institutes INSU and IPEV, the French program SOERE/Great-gases, and the European program FP7/Carbochange.

Table 1: Stations labels, date and locations and attributed hydrological zone. Mixed layer depth (MLD), Depth of the euphotic layer (Ze), Depth of the fluorescence-derived chlorophyll maximum (Chl_{max}) and percentage of chlorophyll located under the mixed layer depth.

Station	Date	Location	Zone	MLD (m)	Ze (m)	Depth of Chl_{max} (m)	% Chl under MLD
5	11/01/2014	42°30'S 52°29'E	SAZ	35	35	20	39
6	12/01/2014	44°60'S 52°06'E	PFZ	52	53	75	73
7	14/01/2014	47°40'S 58°00'E	PFZ	59	58	46	54
8	16/01/2014	48°00'S 60°00'E	PFZ	63	44	44	46
9	17/01/2014	48°30'S 65°01'E	AAZ	70	42	77	58
10	19/01/2014	50°40'S 68°25'E	AAZ	76	38	48	28
11	21/01/2014	56°30'S 62°59'E	AAZ	71	66	61	65
A3	23/01/2014	50°38'S 72°05'E	AAZ	78	37	50	53
12	06/02/2014	46°59'S 72°01'E	PFZ	56	58	70	69
13	06/02/2014	44°59'S 73°20'E	SAZ	39	44	47	50
14	08/02/2014	42°28'S 74°54'E	SAZ	38	49	50	70

Table 2: Sample code (M : mixed layer, T : transition layer, D : 250 m), sampling depth and concentrations of particulate organic carbon (POC), nitrogen (PON) and phosphorous (POP). Nutrient diffusive flux was calculated using a Kz value of 4.5×10^{-5} m^2 s^{-1} in the transition layer (see materials and methods).

Sample	Depth (m)	Particulate stock (µmol L^{-1})				Chlorophyll *a* (µg L^{-1})	Nutrient gradient (µmol m^{-4})			Nutrient diffusive flux (µmol m^{-2} d^{-1})			Brunt-Väisälä Frequency (cycle h^{-1})
		POC	PON	POP	BSi		$Si(OH)_4$	NO_3^-	PO_4^{3-}	$Si(OH)_4$	NO_3^-	PO_4^{3-}	
5M	20	18.60	2.34	0.19	1.07	1.26	0	78	7				3.1
5T	57	3.30	0.47	0.06	0.25	0.20	46	94	1	178	367	6	4.8
5D	250	1.10	0.15	0.02	0.02	0.01	15	35	2				2.3
6M	30	6.00	0.93	0.09	0.17	0.50	0	20	1				2.7
6T	71	5.53	0.85	0.05	0.25	0.67	100	89	7	390	345	25	8.2
6D	250	1.48	0.18	0.02	0.19	0.02	133	37	2				2.5
7M	39	4.85	0.72	0.10	0.16	0.40	37	0	4				2.9
7T	74	2.66	0.41	0.02	0.20	0.41	108	61	2	419	236	8	6.5
7D	249	1.27	0.18	0.02	0.17	0.02	81	20	2				2.2
8M	32	4.56	0.64	0.08	0.10	0.73	18	0	5				1.9
8T	100	4.93	0.80	0.04	0.26	0.37	69	49	3	269	191	10	5.1
8D	250	1.29	0.13	0.02	0.18	0.02	107	15	2				2.8
9M	50	7.25	1.10	0.17	3.19	0.83	27	8	0				2.2
9T	110	5.01	0.73	0.09	4.35	1.04	241	22	4	935	86	16	6.9
9D	250	1.36	0.18	0.02	1.02	0.04	168	37	3				2.9
10M	49	7.79	1.09	0.15	4.91	1.00	12	0	1				2.1
10T	99	3.45	0.42	0.06	3.14	0.69	342	71	6	1328	274	24	5.8
10D	248	1.36	0.17	0.02	0.57	0.03	156	19	2				2.4
11M	49	4.14	0.59	0.15	1.84	0.51	25	31	2				2.7
11T	119	3.46	0.43	0.09	1.52	0.63	143	15	3	556	58	10	4.4
11D	250	0.97	0.10	0.02	0.53	0.03	163	22	1				2.1
12M	40	4.57	0.62	0.07	0.24	0.49	21	18	0				3.3
12T	70	2.96	0.41	0.06	0.29	0.55	64	35	4	250	135	15	6.5
12D	250	1.46	0.15	0.02	0.21	0.03	109	40	1				2.6
13M	21	10.60	1.52	0.13	0.28	0.73	0	0	0				3.4
13T	46	6.77	0.95	0.08	0.37	0.82	71	24	0	277	93	0	8.2
13D	251	1.90	0.25	0.04	0.09	0.02	14	27	1				2.1
14M	20	10.49	1.59	0.15	0.33	0.62	0	0	3				4.1
14T	55	6.81	1.04	0.10	0.65	0.94	64	34	2	251	133	7	6.3
14D	250	1.85	0.20	0.03	0.09	0.04	2	22	1				2.1
A3M	41	9.36	1.47	0.25	4.71	1.10	1	15	0				2.0
A3T	110	8.19	1.31	0.18	5.08	1.20	426	83	6	1655	322	22	6.1
A3D	250	3.39	0.54	0.06	1.50	0.21	142	19	3				2.3

Table 3: Total microplankton cells abundances, total microplankton POC, and relative contribution of each microplanktonic group to the total abundance.

Sample	Total cell abundance (10^3 L^{-1})	Total microplankton POC (µmol L^{-1})	Contribution to total microplankton abundance (%)												
			Empty Diatoms (>100 µm)	Empty Diatoms (<100 µm)	Full Diatoms (>100 µm)	Full Diatoms (<100 µm)	CRS	Naked dinofla-gellate	*Proro-centrum*	Other armored dinofla-gellates	Naked ciliates	Tintinnids	Total diatoms	Total dinoflagellates	Total ciliates
5M	527	13.50	0	2	0	90	0	1	5	0	2	0	92	6	2
5T	25	1.34	1	3	1	60	0	4	25	1	4	1	65	30	5
5D	3	0.19	0	0	0	0	0	5	60	2	34	0	0	66	34
6M	49	3.23	0	5	1	19	0	9	38	0	28	1	24	47	28
6T	40	2.34	0	5	1	23	0	6	41	0	23	1	30	46	24
6D	5	0.16	0	48	0	4	0	3	33	1	11	0	52	37	11
7M	5	1.83	0	4	2	20	0	14	36	0	25	0	25	50	25
7T	8	1.26	0	22	2	20	0	6	34	0	15	0	45	40	15
7D	8	0.13	0	52	0	4	0	3	29	1	12	0	56	32	12
8M	12	2.29	0	1	1	17	0	24	24	0	33	0	19	49	33
8T	10	2.07	0	29	1	23	0	5	28	0	14	0	53	32	15
8D	6	0.14	0	15	0	0	0	5	59	1	20	0	15	65	20
9M	89	4.46	1	19	6	57	0	7	7	0	3	0	83	14	3
9T	104	3.41	1	32	3	51	0	4	6	0	2	0	87	10	2
9D	12	0.19	2	50	0	18	0	12	15	0	3	0	70	27	3
10M	145	4.38	1	18	7	67	0	4	3	0	1	0	92	7	1
10T	77	2.36	2	44	7	34	0	5	6	1	2	0	86	11	2
10D	11	0.11	0	38	0	1	0	16	18	0	26	0	39	34	26
11M	114	2.82	1	17	4	71	0	2	1	0	2	0	94	4	2
11T	75	1.50	1	52	2	33	0	5	4	0	2	0	89	9	2
11D	22	0.14	2	82	0	1	0	8	8	0	0	0	84	16	0
12M	24	2.28	0	15	12	35	0	5	28	0	5	1	61	33	5
12T	16	1.24	0	16	5	28	0	3	32	0	16	0	49	35	16
12D	13	0.14	3	63	1	8	0	1	18	0	6	0	75	19	6
13M	149	6.72	0	4	1	24	0	21	39	1	9	0	30	61	9
13T	77	4.31	0	3	1	48	0	9	26	4	8	0	53	39	8
13D	2	0.23	0	0	0	0	0	17	78	0	6	0	0	94	6
14M	103	6.15	1	0	4	23	0	12	42	7	11	1	28	61	12
14T	72	3.50	1	3	8	63	0	10	15	0	0	0	74	26	0
14D	4	0.13	1	5	2	4	0	18	68	1	1	1	12	87	2
A3M	108	7.29	2	17	13	60	0	3	3	1	2	0	91	7	2
A3T	234	5.75	0	13	8	66	8	1	2	0	1	0	95	3	2
A3D	110	2.89	1	17	0	37	39	2	2	0	1	0	94	4	1

Figures legends

Figure 1: Location of the study in the Indian sector of the Southern Ocean and station map. Satellite-derived surface chlorophyll *a* (MODIS level 3 product, 8 days composite) was averaged from 9 January 2013 to 10 February 2014. Arrows correspond to altimetry-derived geostrophic velocities (AVISO MA-DT daily product) averaged over the same period. Grey lines represent the 500 m and 1000 m isobaths. SAF: Subantarctic Front, PF: Polar Front, SAZ: Subantarctic Zone, PFZ: Polar Frontal Zone, AAZ: Antarctic Zone.

Figure 2: Potential temperature/salinity diagram. a) Colored points denote Si* ($Si(OH)_4 - NO_3^-$) distribution. Circled labels refer to stations. The main water masses identified are specified: SASW: Subantarctic Surface Water, SAMW: Subantarctic Mode Water, AAIW: Antarctic Intermediate Water, AASW: Antarctic Surface Water, WW: Winter Water, CDW: Circumpolar Deep Water, AABW: Antarctic Bottom Water. b) Detailed view for stations of the PFZ and AAZ.

Figure 3: Example of vertical profiles for station 9. a) Potential density anomaly (σ_θ, black line), fluorescence-derived chlorophyll *a* (grey line) and turbulent diffusion coefficient (Kz, black dashed line). b) Vertical profile of nitrate (triangles), phosphate (circles) and silicate (square).

Figure 4: Particulate matter stoichiometry. a) POC:PON versus BSi:POC. b) PON:POP versus BSi:POC. c) Chl:POC versus BSi:POC. Horizontal dashed line is the mean BSi:POC ratio from Quéguiner and Brzezinski (2002) for the Polar Frontal Zone in the Indian sector of the Southern Ocean (0.47). Vertical dashed line are the mean POC:PON and PON:POP ratios for the Southern Ocean from Martiny et al. (2013) (7.4 and 10.6, respectively).

Figure 5: Dendrogram of the hierarchical clustering (UPGMA agglomeration) based on the Bray-Curtis distance calculated on raw microplankton abundances. Capital letters categorize the groups referred to in the text.

Figure 6: Fraction of empty diatoms for a) mixed layer samples, b) transition layer samples and c) 250 m samples. Black dots represent the fraction of total empty diatoms to the sum of full and empty diatom frustules. Patterned bars refer to the fraction of a diatom group as specified in the legend.

Figure 7: Microplankton POC partitioning for a) mixed layer samples, b) transition layer samples and c) 250 m samples. Patterned bars refer to the contribution of a microplankton group as specified in the legend.

Figure 8: Projection of samples, main microplankton groups and biogeochemical factors (particulate matter stoichiometry and major nutrients diffusive fluxes) on the first two axes of the canonical correspondence analysis (CCA).

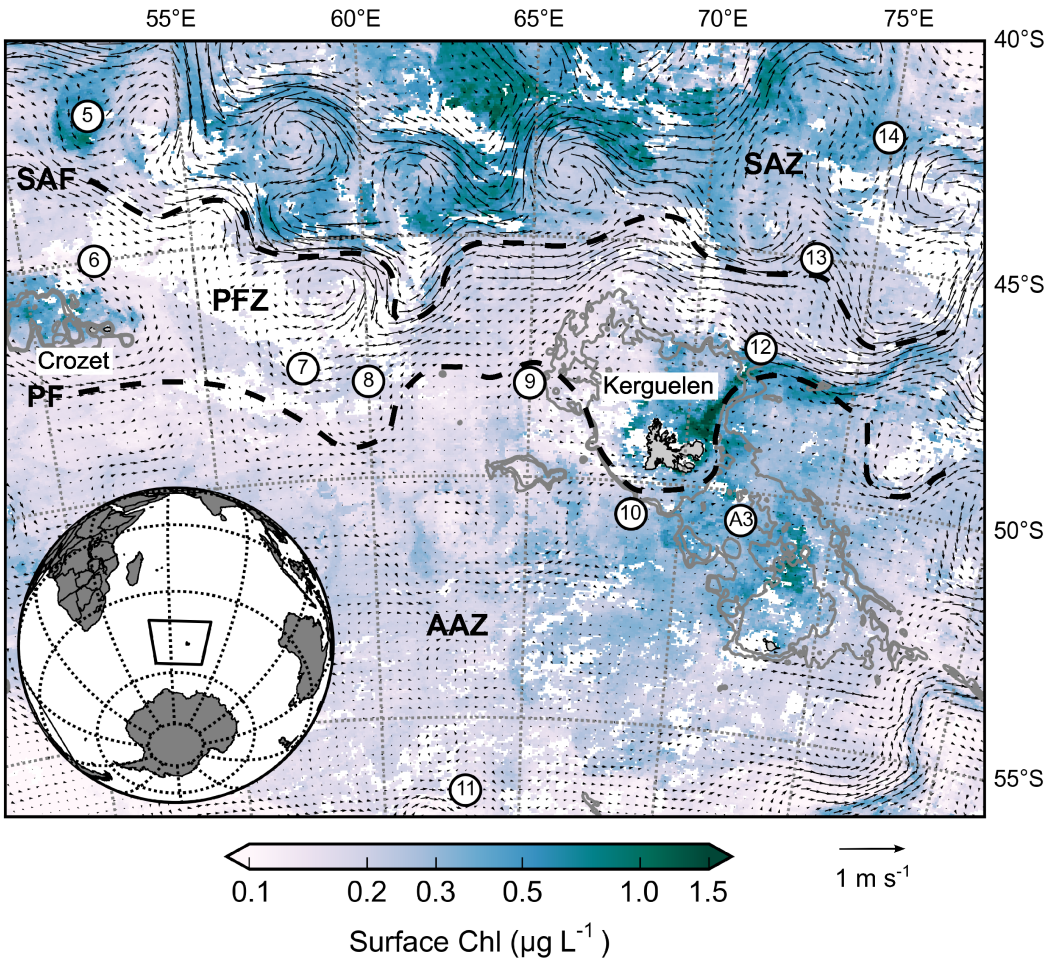
55°E
60°E
65°E
70°E
75°E
40°S
45°S
50°S
55°S
SAF
PFZ
PF
SAZ
AAZ
Crozet
Kerguelen
A3
5
6
7
8
9
10
11
12
13
14
0.1
0.2
0.3
0.5
1.0
1.5
Surface Chl (µg L-1)
1 m s-1

Figure 1.

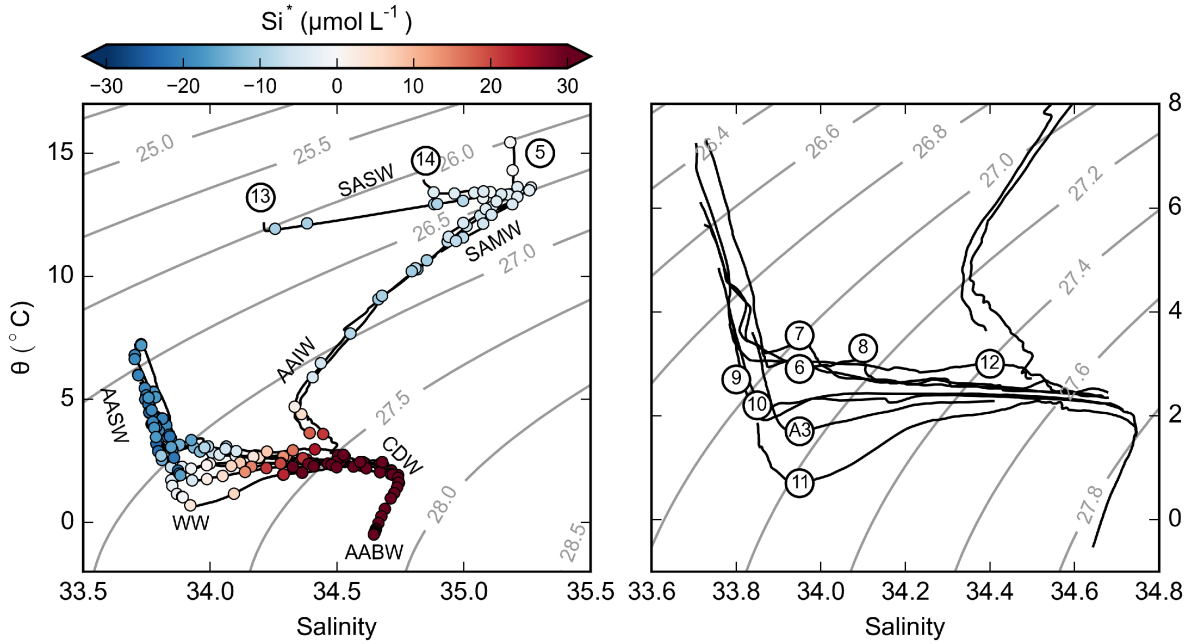

Figure 2.

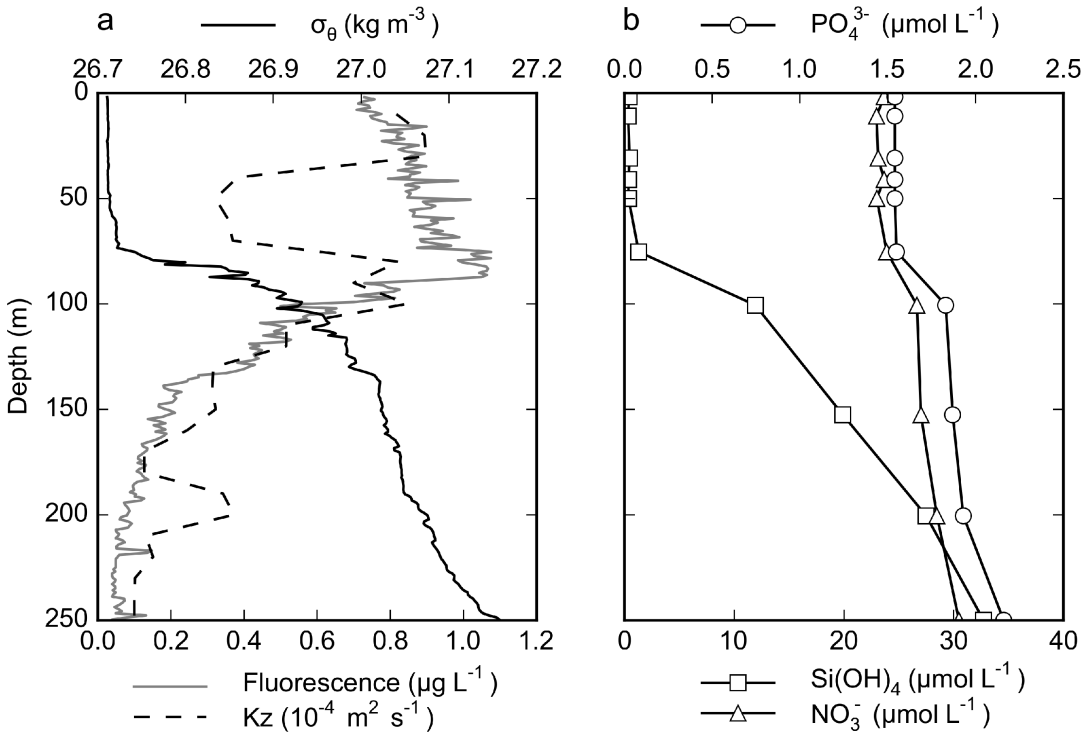

Figure 3.

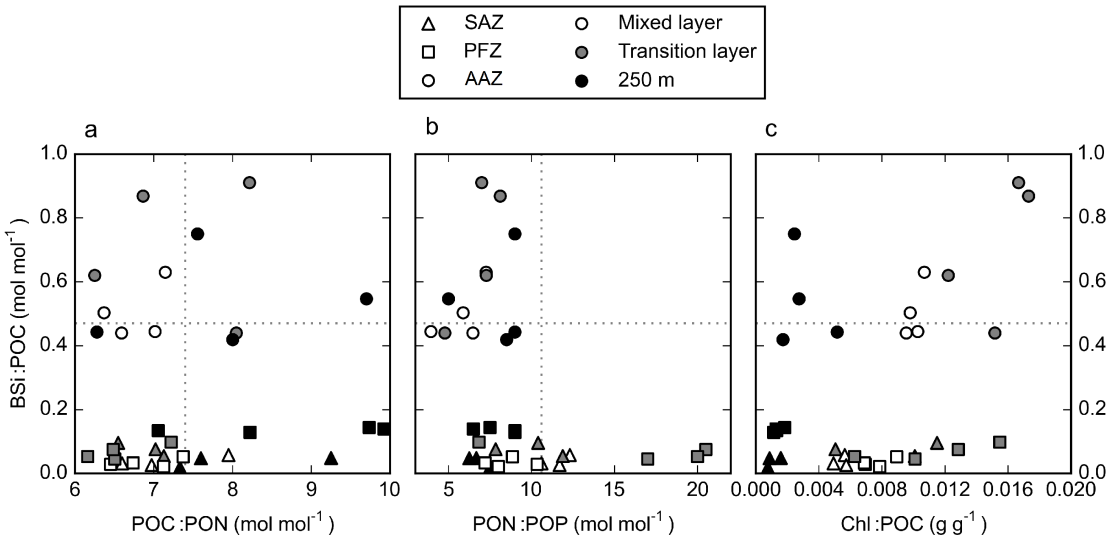

Figure 4.

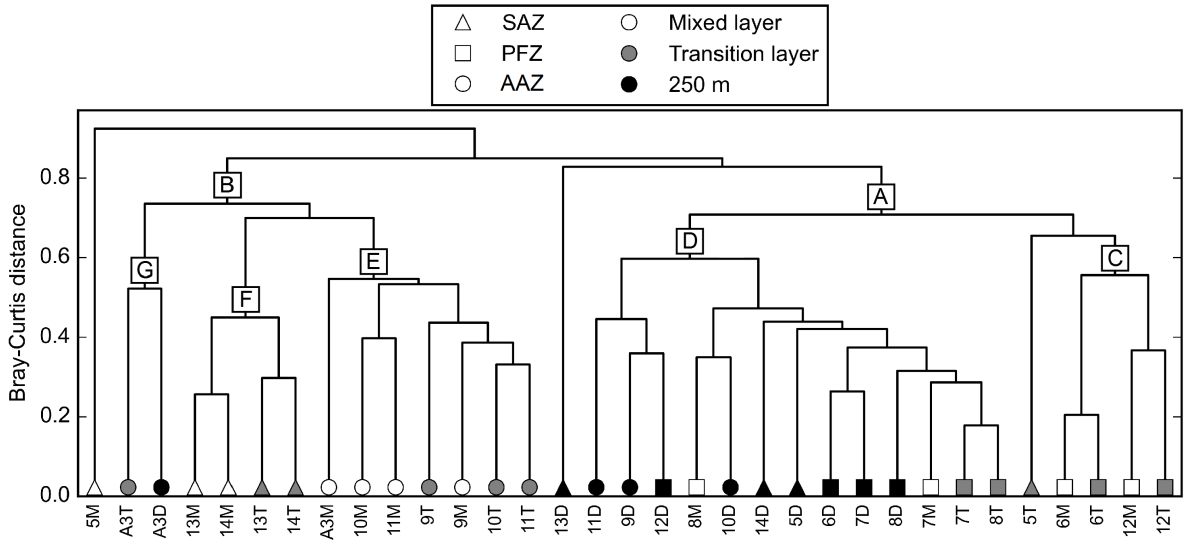

Figure 5.

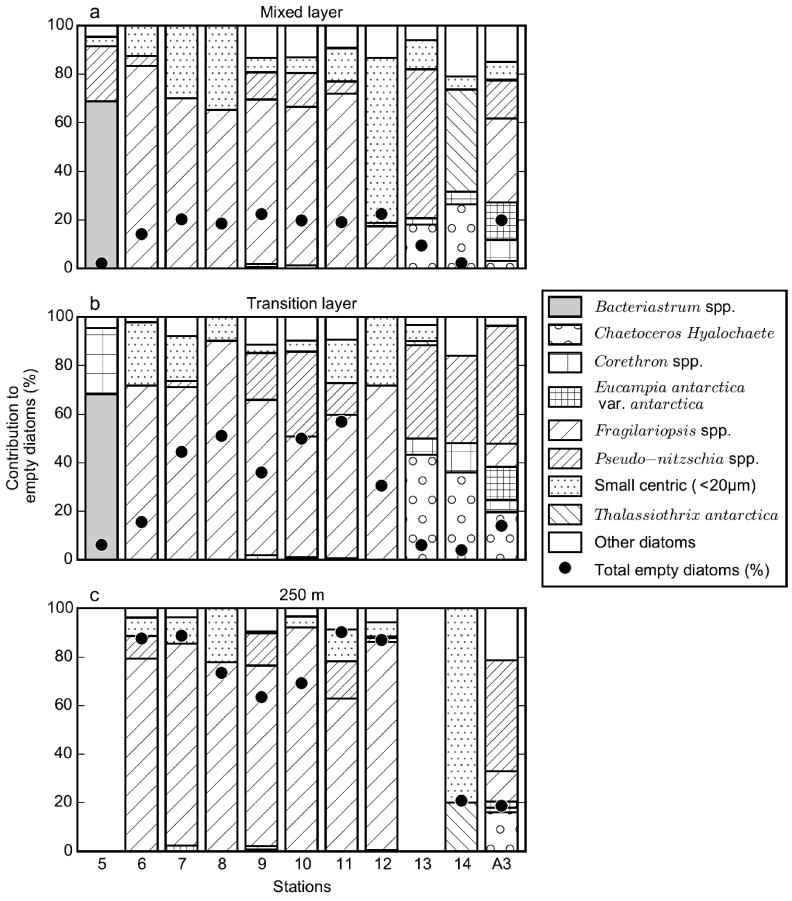
a
Mixed layer
b
Transition layer
c
250 m
Contribution to empty diatoms (%)
100
80
60
40
20
0
5
6
7
8
9
10
11
12
13
14
A3
Stations
Bacteriastrum spp.
Chaetoceros Hyalochaete
Corethron spp.
Eucampia antarctica var. antarctica
Fragilariopsis spp.
Pseudo–nitzschia spp.
Small centric (<20µm)
Thalassiothrix antarctica
Other diatoms
Total empty diatoms (%)

Figure 6.

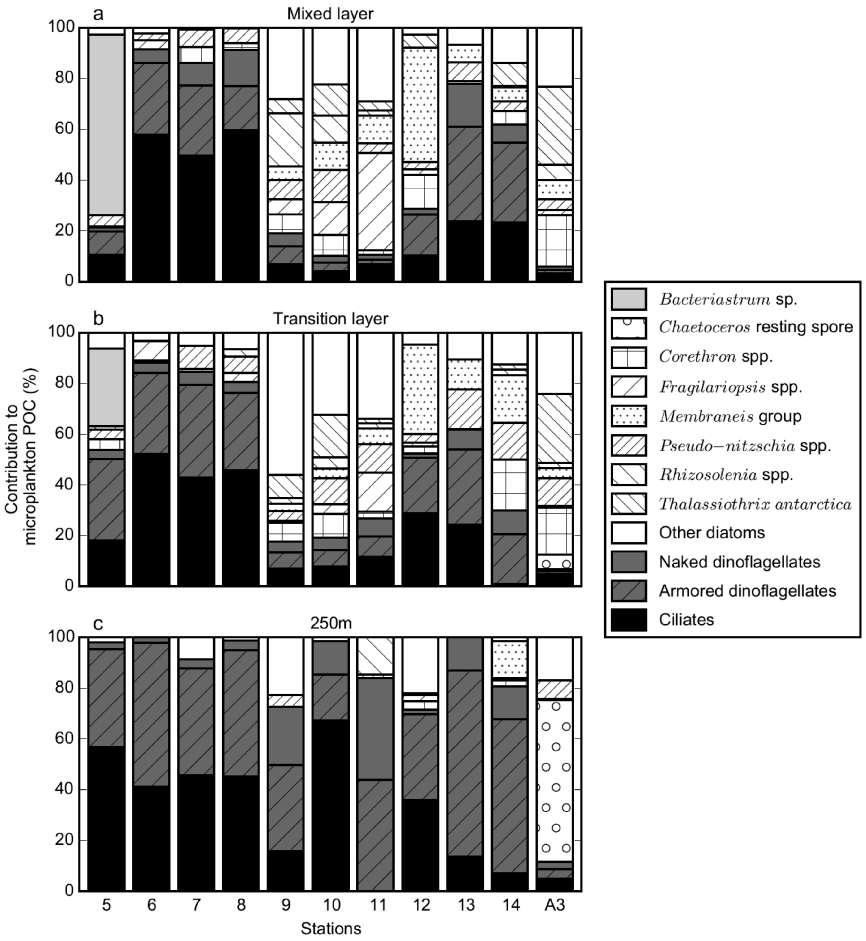
a
Mixed layer
b
Transition layer
c
250m
Contribution to microplankton POC (%)
0
20
40
60
80
100
5
6
7
8
9
10
11
12
13
14
A3
Stations
Bacteriastrum sp.
Chaetoceros resting spore
Corethron spp.
Fragilariopsis spp.
Membraneis group
Pseudo−nitzschia spp.
Rhizosolenia spp.
Thalassiothrix antarctica
Other diatoms
Naked dinoflagellates
Armored dinoflagellates
Ciliates

Figure 7.

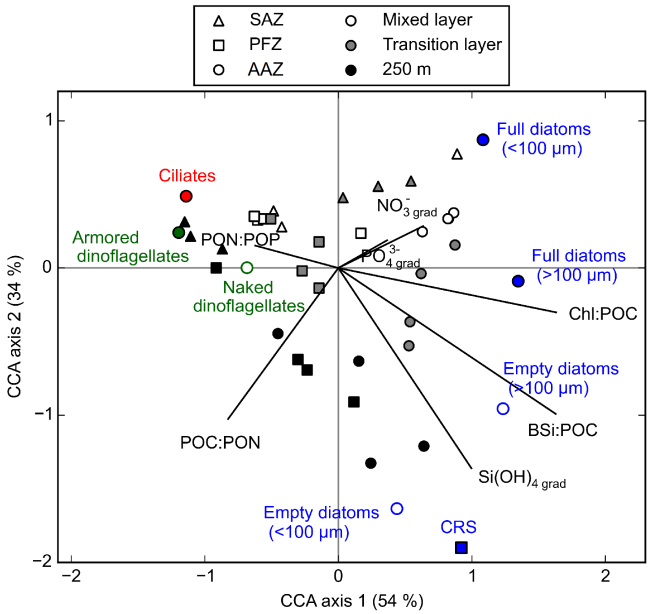
SAZ
PFZ
AAZ
Mixed layer
Transition layer
250 m
Full diatoms (<100 µm)
Ciliates
$NO^-_{3\ grad}$
Armored dinoflagellates
PON:POP
$PO^{3-}_{4\ grad}$
Full diatoms (>100 µm)
Naked dinoflagellates
Chl:POC
Empty diatoms (>100 µm)
BSi:POC
POC:PON
$Si(OH)_{4\ grad}$
Empty diatoms (<100 µm)
CRS
CCA axis 2 (34 %)
CCA axis 1 (54 %)
1
0
−1
−2
−2
−1
0
1
2

Figure 8.